

**Nitrate deposition and preservation in the snowpack along a traverse
from coast to the ice sheet summit (Dome A) in East Antarctica**

Guitao Shi^{1,2}, Meredith G. Hastings³, Jinhai Yu^{2,4}, Tianming Ma^{2,5}, Zhengyi Hu²,
Chunlei An², Chuanjin Li⁶, Hongmei Ma², Su Jiang², and Yuansheng Li²

¹ Key Laboratory of Geographic Information Science (Ministry of Education) and School of
Geographic Sciences, East China Normal University, Shanghai 200241, China

² Key Laboratory for Polar Science of State Oceanic Administration, Polar Research Institute of China,
Shanghai 200062, China

³ Department of Earth, Environmental and Planetary Sciences and Institute at Brown for Environment
and Society, Brown University, Providence, Rhode Island 02912, USA.

⁴ School of Geographic and Oceanographic Sciences, Nanjing University, Nanjing 210023, China

⁵ School of Ocean and Earth Science, Tongji University, Shanghai 200092, China

⁶ The State Key Laboratory of the Cryospheric Sciences, Northwest Institute of Eco-Environment and
Resources, Chinese Academy of Sciences, Lanzhou 730000, China

Correspondence to: G. Shi (gt_shi@163.com) and M.G. Hastings (meredith_hastings@brown.edu)

Abstract. Antarctic ice core nitrate (NO_3^-) can provide a unique record of the atmospheric reactive nitrogen cycle. However, the factors influencing the deposition and preservation of NO_3^- at the ice sheet surface must first be understood. Therefore, an intensive program of snow and atmospheric sampling was made on a traverse from the coast to the ice sheet summit, Dome A, East Antarctica. Snow samples in this observation include 120 surface snow samples (top ~3 cm), 20 snowpits with depths of 150 to 300 cm, and 6 crystal ice samples (the topmost needle like layer on Dome A plateau). The main purpose of this investigation is to characterize the distribution pattern and preservation of NO_3^- concentrations in the snow in different environments. Results show that an increasing trend of NO_3^- concentrations with distance inland is present in surface snow, and NO_3^- is extremely enriched in the crystal ice (with a maximum of $16.1 \mu\text{eq L}^{-1}$). NO_3^- concentration profiles for snowpits vary between coastal and inland sites. On the coast, the deposited NO_3^- was largely preserved, and the archived NO_3^- fluxes are dominated by snow accumulation. The relationship between the archived NO_3^- and snow accumulation rate can be well depicted by a linear model, suggesting a homogeneity of atmospheric NO_3^- levels. It is estimated that dry deposition contributes 27-44 % of the archived NO_3^- fluxes, and the dry deposition velocity and scavenging ratio for NO_3^- was relatively constant near the coast. Compared to the coast, the inland snow shows a relatively weak correlation between archived NO_3^- and snow accumulation, and the archived NO_3^- fluxes were more concentration dependent. The relationship between NO_3^- and coexisting ions (nssSO_4^{2-} , Na^+ and Cl^-) was also investigated, and the results show a correlation between nssSO_4^{2-} (fine aerosol particles) and NO_3^- in surface snow, while the correlation between NO_3^- and Na^+ (mainly associated with coarse aerosol particles) is not significant. In inland snow, there were no significant relationships found between NO_3^- and the coexisting ions, suggesting a dominant role of NO_3^- recycling in determining the concentrations.

1 Introduction

As the major sink of atmospheric nitrogen oxides ($\text{NO}_x = \text{NO}$ and NO_2), nitrate (NO_3^-) is one of the major chemical species measured in polar snow and ice. The measurements of NO_3^- in ice cores may offer potential for understanding the complex atmospheric nitrogen cycle as well as oxidative capacity of the atmosphere through time (Legrand and Mayewski, 1997; Alexander et al., 2004; Hastings et al., 2009; Geng et al., 2017). However, the sources, transport pathways, and preservation of NO_3^- in Antarctic snowpack are still not well understood, hampering the interpretation of ice core NO_3^- records.

The accumulation of NO_3^- in snow is associated with various environmental factors and continental, tropospheric and stratospheric sources could influence NO_3^- concentrations (Legrand and Kirchner, 1990; McCabe et al., 2007; Wolff et al., 2008; Lee et al., 2014). In surface snow, NO_3^- levels are thought to be linked with snow accumulation rate, and higher values are usually present in areas with low accumulation, e.g., East Antarctic plateaus (Qin et al., 1992; Erbland et al., 2013; Traversi et al., 2017). Unlike sea salt related ions (e.g., chloride (Cl^-), sodium (Na^+), and occasionally sulfate (SO_4^{2-})), NO_3^- does not usually show an elevated level in coastal Antarctic snow (Mulvaney and Wolff, 1994; Bertler et al., 2005; Frey et al., 2009), suggesting a negligible contribution from sea salt aerosols. However, the marine emissions of alkyl NO_3^- , particularly methyl and ethyl NO_3^- , produced in surface oceans by microbiological and/or photochemical processes, are thought to be a possible contribution to Antarctic NO_3^- (Jones et al., 1999; Liss et al., 2004). At Halley station in coastal Antarctica, significant concentrations of organic nitrates (peroxyacetyl nitrate (PAN) and alkyl NO_3^-) were observed in the lower atmosphere (Jones et al., 2011). Organic nitrates dominated the NO_y (sum of reactive nitrogen oxide compounds) budget during the winter, and were on par with inorganic nitrate compounds during the summer. Although not a direct source of snowpack nitrate, organic nitrates could act as source of NO_x to coastal Antarctica that would ultimately contribute to NO_3^- within the snowpack (Jones et al., 2011).

While industrial and/or agricultural emissions have contributed to increasing NO_3^- levels in Greenland snow and ice over recent decades to hundreds of years, the anthropogenic contribution to Antarctic NO_3^- is less clear (Mayewski and Legrand, 1990; Hastings et al., 2009; Felix and Elliott, 2013; Geng et al., 2014). Lightning and NO_x produced in the lower stratosphere have long been thought to play a major role (Legrand et al., 1989; Legrand and Kirchner, 1990). Recently, adjoint model simulations proposed that tropospheric transport of NO_3^- from mid-low latitude NO_x sources is an important source to the Antarctic year round, though less so in austral spring/summer (Lee et al., 2014). A recent treatment of NO_3^- in snow in the same global chemical transport model suggests that the recycling of NO_3^- and/or transport of NO_x due to photolysis of NO_3^- in the surface snow layer is important in determining summertime concentrations (Zatko et al., 2016). The stratospheric inputs of NO_3^- are thought to result from N_2O oxidation to NO , then formation of NO_3^- that is deposited via polar stratospheric cloud (PSC) sedimentation (Legrand et al., 1989; Legrand and Kirchner, 1990). The late winter/early spring secondary maximum of NO_3^- observed in the atmosphere at coastal and inland locations has been attributed to the stratospheric source based on the NO_3^- stable isotopic composition (Legrand et al., 1989; Savarino et al., 2007; Frey et al., 2009). At some sites, the snow/ice core NO_3^- concentrations were found to be linked with regional atmospheric circulation (e.g., sea level pressure gradient; Goodwin et al., 2003; Russell et al., 2006). In general, atmospheric circulation appears not to affect snow NO_3^- concentrations directly, but indirectly through an influence on the air mass transport and/or snow accumulation rate (Russell et al., 2004; Russell et al., 2006). In addition, while some

studies suggested that snow/ice NO_3^- is possibly linked with extraterrestrial fluxes of energetic particles and solar irradiation, with solar flares corresponding to NO_3^- spikes (Zeller et al., 1986; Smart et al., 2014), other observations and recent modeling studies have established that there is not a clear connection between solar variability and NO_3^- concentrations (Legrand et al., 1989; Legrand and Kirchner, 1990; Wolff et al., 2008; Wolff et al., 2012; Duderstadt et al., 2014; Duderstadt et al., 2016; Wolff et al., 2016). However, the potential link between the long-term (e.g., centennial to millennial time scales) variability of NO_3^- and solar cycles may be present at some locations (Traversi et al., 2012). In summary, factors influencing NO_3^- levels in snow/ice are complicated, and the significance of the relationship between NO_3^- and controlling factors varies temporally and spatially.

Gas phase and snow concentration studies, and recent isotopic investigations and modeling have shown that NO_3^- , particularly in snow on the Antarctic plateau, is a combination of deposition of HNO_3 and post-depositional loss or recycling of NO_3^- (e.g., R  hlisberger et al., 2002; Davis et al., 2004; Dibb et al., 2004; Erbland et al., 2013; Erbland et al., 2015; Shi et al., 2015; Bock et al., 2016; Zatko et al., 2016). Based upon a suite of isotopic studies in the field and laboratory, it has been demonstrated that under cold, sunlit conditions ultraviolet photolysis dominates NO_3^- post-depositional processing, whereas HNO_3 volatilization may become more important at warmer temperatures $> -20^\circ\text{C}$ (R  hlisberger et al., 2002; Frey et al., 2009; Erbland et al., 2013; Berhanu et al., 2015). In snowpack, the solar radiation decreases exponentially, with attenuation described in terms of an e -folding depth (z_e) where the actinic flux is reduced to 37 % (i.e., $1/e$) of the surface value. Thus, about 95 % of snowpack photochemistry is expected to occur above the depth of three times z_e (Warren et al., 2006). Field measurements at Dome C on the East Antarctic plateau suggest a z_e of 10 to 20 cm (France et al., 2011), and the depth is dependent upon the concentration of impurities contained in the snow (Zatko et al., 2013). In the inland regions with low snow accumulation rates, particularly on the East Antarctic plateaus, photolysis has been shown to lead to significant post-depositional loss of NO_3^- , demonstrated by significant enrichment in ^{15}N of snow NO_3^- (i.e., high $\delta^{15}\text{N}$) (Frey et al., 2009; Erbland et al., 2013; Berhanu et al., 2015; Erbland et al., 2015; Shi et al., 2015), as well as a decrease in $\delta^{18}\text{O}$ and $\Delta^{17}\text{O}$ due to reformation of NO_3^- in the condensed phase (Erbland et al., 2013; Shi et al., 2015 and references therein). The transport and recycling of NO_x sourced from photolysis of snow NO_3^- in the summertime has been invoked to model the distribution of snowpack NO_3^- across the Antarctic plateau (Zatko et al., 2016). However, snow physical characteristics play a crucial role in NO_3^- deposition and preservation. For instance, summertime concentrations in the surface skin layer of snow (the uppermost ~4 mm) can be explained as the result of co-condensation of HNO_3 and water vapour, with little to no photolytic loss in this microlayer (Bock et al., 2016). The combination of concentration and isotopic studies, along with physical aspects of the snow, could lead to the reconstruction and interpretation of atmospheric NO_3^- over time (e.g., Erbland et al., 2015; Bock et al., 2016), if there is detailed understanding of the NO_3^- deposition and preservation in different environments in Antarctica.

The effects of volatilization of NO_3^- are uncertain, given that one field experiment suggests that this process is an active player in NO_3^- loss (17 % (-30°C) to 67 % (-10°C) of NO_3^- lost after two weeks' physical release experiments; Erbland et al., 2013), while other laboratory and field studies show that volatilization plays a negligible role in NO_3^- loss (Berhanu et al., 2014; Berhanu et al., 2015). Further investigations are needed to quantify the effects of volatilization for a better understanding of NO_3^- preservation in snow/ice. Based on z_e , NO_3^- at deeper depths in Antarctic snow (e.g., $> 100\text{ cm}$), well beyond the snow photic zone, may be taken as the archived fraction. Thus, NO_3^- in deeper snow possibly provides an opportunity to investigate the archived fraction and potential influencing factors

(e.g., snow accumulation rate). Given that an extensive array of ice core measurements is unavailable in most of Antarctica, the deeper snowpits (with depth > 100 cm) may offer a useful way to investigate the archived NO_3^- .

In the atmosphere in Antarctica, particularly during spring and summer, NO_3^- is found to be mainly in the form of gas phase HNO_3 , with NO_3^- concentration several times higher in gas phase than in the particulate phase (Piel et al., 2006; Legrand et al., 2017b; Traversi et al., 2017). During post-depositional processes, the uptake of gaseous HNO_3 is thought to be important in NO_3^- concentrations in surface snow layers (Udisti et al., 2004; Traversi et al., 2014; Traversi et al., 2017). Due to the high concentration in summer, HNO_3 appears to play an important role in acidifying sea-salt particles, possibly accounting for the presence of NO_3^- in the particulate phase in summer (Jourdain and Legrand, 2002; Legrand et al., 2017b; Traversi et al., 2017). It is noted that the significant increase of NO_3^- during the cold periods (e.g., Last Glacial Maximum) could be associated with its attachment to dust aerosol, instead of formation of gas phase HNO_3 (Legrand et al., 1999; Wolff et al., 2010).

To date, investigations on spatial and temporal patterns of snow NO_3^- have been performed on several traverses in Antarctica (e.g., 1990 International Trans-Antarctica Expedition, and DDU to Dome C; Qin et al., 1992; Bertler et al., 2005; Frey et al., 2009; Erbland et al., 2013; Pasteris et al., 2014), but these provide an uneven distribution of snow NO_3^- concentrations and leave large regions un-sampled (e.g., Lambert Glacier basin and Dome A plateau). Over the past few decades, while several glaciological observations have been carried out on the Chinese inland Antarctic traverse route from Zhongshan to Dome A, East Antarctica (Hou et al., 2007; Ding et al., 2010; Ma et al., 2010; Ding et al., 2011; Li et al., 2013; Shi et al., 2015), the data on snow chemistry are still rare, particularly detailed information on NO_3^- . From 2009 to 2013, we therefore conducted surface snow and snowpit sampling campaigns along the traverse route, with the main objectives to (1) describe NO_3^- distribution in surface snow and snowpits, (2) characterize the relationship between archived NO_3^- and snow accumulation rate, and (3) examine the potential effects of coexisting ions on NO_3^- preservation. The results of this study may help to better understand NO_3^- deposition and preservation in the snowpack, which is critical to the interpretation of ice core NO_3^- records.

2 Methodology

2.1 Study area (Zhongshan to Dome A traverse)

The Zhongshan to Dome A CHINARE (Chinese National Antarctic Research Expedition) inland traverse is an important leg of the ITASE (International Trans-Antarctic Scientific Expedition). The traverse is in the Indian Ocean sector of East Antarctica, passing through the Lambert Glacier, the largest glacier in Antarctica. In January 1997 the first Chinese Antarctic inland expedition reached an area ~300 km from the coast; in January 1998 the traverse was extended to 464 km, and in December 1998, to the Dome A area ~1100 km from the coast. In the austral 2004/2005 summer for the first time, the traverse extended to the ice sheet summit, Dome A, a total distance of ~1260 km. In January 2009, the Chinese inland research base, Kunlun station (80°25'1.7"S and 77°6'58.0"E, 4087 m above mean sea level), was established at Dome A, mainly aimed at deep ice core drilling and astronomical observations. Now, Kunlun base is a summer station, and the CHINARE team typically conducts an annual inland traverse from the coastal Zhongshan station to Dome A.

In January 2010, the Dome A deep ice core project was started, and the construction of basic infrastructure (including drill trench and scientific workroom) took 4 summer seasons. The deep ice

core drilling began in January 2013, and in total 801 m ice core was recovered by the 2016/2017 season. The investigation of NO_3^- deposition and preservation in the snowpack will be of help to the interpretation of Dome A deep ice core NO_3^- records.

2.2 Sample collection

During the 2010/2011 CHINARE, surface snow samples (the topmost ~3 cm) were collected at an interval of ~10 km along the traverse route from Zhongshan to Dome A, using 3.0 cm diameter high-density polyethylene (HDPE) bottles (volume = 100 ml). The bottles were pre-cleaned with Milli-Q ultrapure water (18.2 M Ω), until electrical conductivity of the water stored in bottles (> 24 h) decreased to <0.5 $\mu\text{S cm}^{-1}$. Then, the bottles were dried under a class 100 super clean hood at 20 °C. Immediately after the drying procedure, the bottles were sealed in clean PE bags that were not opened until the field sampling started. At each sampling site (typically > 500 m away from the traverse route), the bottles were pushed into surface snow layers in the windward direction. In total, 120 surface snow samples were collected. In addition, at each sampling site, the upper snow density (~10 cm) was measured using a density scoop with a volume of 1000 cm^3 . As the field blanks, pre-cleaned bottles filled with Milli-Q water were taken to the field and treated to the same conditions as field samples ($n = 3$).

On the Dome A plateau, the snow is soft and non-cohesive, and morphology of the surface snow is different from other areas on the traverse, with a needle ice crystal layer extensively developed, in particular on the sastrugi (Fig. S1 in supporting information). The depth of the needle-like crystal ice layer (referred to as “crystal ice” in the following context) is generally < 1.0 cm. In order to investigate air-snow transfer of NO_3^- in this uppermost ~1 cm layer, the crystal ice was collected using a clean HDPE scoop, and then poured into clean wide mouth HDPE bottles. Approximately 30 g of crystal ice was collected for each sample. In total, 6 crystal ice samples were collected on the traverse near Dome A plateau.

In addition to surface snow, snowpit samples were collected during CHINARE inland traverse campaigns in 2009/2010, 2010/2011, and 2012/2013. The snowpits were excavated manually, and the snow wall in the windward direction was scraped clean and flat with a clean HDPE scraper. Then the bottles were pushed horizontally into the snow wall. Snowpit samples were collected from the base towards the top layer along a vertical line. During the sampling process, all personnel wore PE gloves and facemasks to minimize potential contamination. Note that the snowpits are generally > 1 km from the traverse route to avoid possible contamination from the expedition activities. The full information about individual snowpits, including location, distance from the coast, elevation, snowpit depth, sampling resolution, collection date, and annual snow accumulation rate, is summarized in Table 1. All together, 20 snowpits (SP1 to SP20 in Fig. 2, with SP20 corresponding to the location of Kunlun station at Dome A) as 1741 snow samples, were collected.

To support understanding of the air-snow transfer of NO_3^- on the traverse, atmospheric NO_3^- was collected on glass fiber filters (Whatman G653) using a high volume air sampler (HVAS), with a flow rate of ~1.0 $\text{m}^3 \text{min}^{-1}$ for 12-15 hr, during the inland traverse campaign in 2015/2016. The NO_3^- collected on glass fiber filters are expected to equal the sum of particulate NO_3^- and gaseous HNO_3 , based upon previous investigations in East Antarctica (Savarino et al., 2007; Frey et al., 2009; Erbland et al., 2013). In total, 34 atmospheric samples were collected on the traverse. In addition, two field blanks were collected from filters installed in the HVAS without pumping and treated as samples thereafter. Detailed information about the atmospheric sampling is presented in Table S1 in supporting

information.

After sample collection, all filters and snow samples were sealed in clean PE bags and preserved in clean thermal insulated boxes. All of the samples were transported to the laboratory under freezing conditions ($< -20^{\circ}\text{C}$).

2.3 Sample analysis

In the laboratory, three quarters of individual filters were cut into pieces using pre-cleaned scissors that were rinsed between samples, placed in ~ 100 ml of Milli-Q water, ultrasonicated for 40 min and leached for 24 hr under shaking. The sample solutions were then filtered through $0.22\ \mu\text{m}$ ANPEL PTFE filters for concentration analysis. Snow samples were melted in the closed sampling bottles on a super clean bench (class 100) before chemical measurements. Analyses of Na^+ , NH_4^+ , K^+ , Mg^{2+} , Ca^{2+} , Cl^- , NO_3^- and SO_4^{2-} were performed using a Dionex ICS-3000 ion chromatography system. The column used for cation analysis (Na^+ , NH_4^+ , K^+ , Mg^{2+} and Ca^{2+}) was a Dionex column CS12 (2×250 mm), with a guard column CG12 (2×50 mm); while the anions (Cl^- , NO_3^- and SO_4^{2-}) were analyzed using a Dionex column AS11 (2×250 mm) with a guard column AG11 (2×50 mm). The eluent for cations was 18.0 mM methanesulfonic acid (MSA), and the gradient elution method was employed for anion analysis, with eluent of potassium hydroxide (KOH). More details on this method are described in a previous report (Shi et al., 2012). During sample analysis, duplicated samples and field blanks were

synchronously analyzed. The pooled standard deviation (σ_p , $\sigma_p = \sqrt{\sum_{i=1}^k (n_i - 1) s_i^2 / \sum_{i=1}^k (n_i - 1)}$), where n_i and s_i^2 are the size and variance of the i th samples respectively, and k is the total number of sample sets) of all replicate samples run at least twice in two different sample sets is 0.019 (Cl^-), 0.023 (NO_3^-), 0.037 (SO_4^{2-}), 0.022 (Na^+), 0.039 (NH_4^+), 0.006 (K^+), 0.006 (Mg^{2+}) and 0.006 (Ca^{2+}) $\mu\text{eq L}^{-1}$ respectively ($n = 65$ pairs of samples). Ion concentrations in field blanks ($n = 3$) are generally lower than the detection limit (DL, 3 standard deviations of water blank in the laboratory).

For Antarctic snow samples, the concentrations of H^+ are usually not measured directly, but deduced from the ion-balance disequilibrium in the snow. Here, H^+ concentration is calculated through ion balance.

$$[\text{H}^+] = [\text{Cl}^-] + [\text{NO}_3^-] + [\text{SO}_4^{2-}] - [\text{Na}^+] - [\text{NH}_4^+] - [\text{Mg}^{2+}] - [\text{Ca}^{2+}] \text{ (Eq. 1)},$$

where ion concentrations are in $\mu\text{eq L}^{-1}$. In addition, the non-sea salt fractions of SO_4^{2-} (nssSO_4^{2-}) and Cl^- (nssCl^-) can be calculated from the following expressions, by assuming Na^+ exclusively from sea salt (in $\mu\text{eq L}^{-1}$).

$$[\text{nssSO}_4^{2-}] = [\text{SO}_4^{2-}] - 0.12 \times [\text{Na}^+] \text{ (Eq. 2)},$$

$$[\text{nssCl}^-] = [\text{Cl}^-] - 1.17 \times [\text{Na}^+] \text{ (Eq. 3)}.$$

It is noted that SO_4^{2-} fractionation (the precipitation of mirabilite ($\text{Na}_2\text{SO}_4 \cdot 10\text{H}_2\text{O}$)) may introduce a bias in nssSO_4^{2-} , particularly during the winter half year (Wagenbach et al., 1998a).

3 Results

3.1 NO_3^- concentration in surface snow

Concentrations of NO_3^- in surface snow are shown in Fig. 1, ranging from 0.6 to 5.1 $\mu\text{eq L}^{-1}$, with a mean of 2.4 $\mu\text{eq L}^{-1}$. One standard deviation (1σ) of NO_3^- concentration in surface snow is 1.1 $\mu\text{eq L}^{-1}$, with coefficient of variation (Cv , 1σ over mean) of 0.5, indicating a moderate spatial variability. On the coastal ~ 450 km, NO_3^- shows a slightly increasing trend towards the interior, with low variability, while

NO₃⁻ concentrations are higher in the inland region, with a large fluctuation. It is notable that in the area ~800 km from the coast, where snow accumulation is relatively high, NO₃⁻ concentrations decrease to < 2.0 µeq L⁻¹, comparable to the values on the coast. Near the Dome A plateau (> 1000 km from coast), there is a tendency for higher NO₃⁻ concentrations (> 5.0 µeq L⁻¹). Similarly, atmospheric NO₃⁻ concentrations increase from the coast towards the plateau, ranging from 8 to 183 ng m⁻³ (mean = 55 ng m⁻³) (Fig. 1).

The percentage that surface snow NO₃⁻ contributes to total ions (i.e., total ionic strength, sum of Na⁺, NH₄⁺, K⁺, Mg²⁺, Ca²⁺, Cl⁻, NO₃⁻, SO₄²⁻ and H⁺, in µeq L⁻¹) varies from 6.7 to 37.6 % (mean = 27.0 %; Fig. S2 in supporting information), with low values near the coast and high percentages on the plateau. A strong relationship was found between NO₃⁻ and the total ionic strength in surface snow ($R^2 = 0.55$, $p < 0.01$).

In the crystal ice, the means (ranges) of Cl⁻, NO₃⁻, SO₄²⁻, Na⁺, NH₄⁺, K⁺, Mg²⁺, Ca²⁺ and H⁺ concentrations are 0.98 (0.62 – 1.27), 10.40 (8.35 – 16.06), 1.29 (0.87 – 2.13), 0.27 (0.21 – 0.33), 0.24 (0.03 – 0.56), 0.05 (0.03 – 0.08), 0.18 (0.15 – 0.22), 0.18 (0.05 – 0.57) and 11.75 (9.56 – 18.12) µeq L⁻¹, respectively. H⁺ and NO₃⁻ are the most abundant species, accounting for 46.4 and 41.0 % of the total ions, followed by SO₄²⁻ (5.1 %) and Cl⁻ (3.9 %). The other 5 cations, Na⁺, NH₄⁺, K⁺, Mg²⁺ and Ca²⁺, only represent 3.6 % of the total ion budget. A significant linear relationship was found between NO₃⁻ and the total ionic strength ($R^2 = 0.99$, $p < 0.01$), possibly suggesting that NO₃⁻ is the species controlling ion abundance by influencing acidity of the crystal ice (i.e., H⁺ levels). In comparison with surface snow, concentrations of H⁺ and NO₃⁻ are significantly higher in crystal ice (Independent Samples T Test, $p < 0.01$), while concentrations of Cl⁻, SO₄²⁻, Na⁺, NH₄⁺, K⁺, Mg²⁺ and Ca²⁺ are comparable in the two types of snow samples (Fig. S2 in supporting information). To date, the information on the chemistry of ice crystal is rather limited but data from the so-called skin layer at Dome C (top ~4 mm snow), where NO₃⁻ concentrations are in the range of 9 – 22 µeq L⁻¹ in summertime (Erbland et al., 2013), are generally comparable to our observations.

NO₃⁻ concentrations in surface snow have been widely measured across Antarctica (Fig. 2), and the values vary from 0.2 to 12.9 µeq L⁻¹, with a mean of 2.1 µeq L⁻¹ ($n = 594$, $1\sigma = 1.7$ µeq L⁻¹) and a median of 1.4 µeq L⁻¹. Most of the data (87 %) fall in the range of 0.5 - 4.0 µeq L⁻¹, and only 7 % of the values are above 5.0 µeq L⁻¹, mainly distributed on the East Antarctic plateaus. Spatially, NO₃⁻ concentrations show an increasing trend with distance inland, and the values are higher in East than in West Antarctica. Overall, this spatial pattern is opposite to that of the annual snow accumulation rate (Arthern et al., 2006), i.e., low (high) snow accumulation corresponds to high (low) NO₃⁻ concentrations. It is difficult to compare with NO₃⁻ concentrations derived from the “upper snow layer” in different studies because each study sampled a different depth (Fig. 2), e.g., 2 - 10 cm for DDU-Dome C traverse (Frey et al., 2009; Erbland et al., 2013), 25 cm for the 1989-1990 International Trans-Antarctica Expedition (Qin et al., 1992) and 3 cm for this study. The different sampling depths can result in large differences in NO₃⁻ concentration, especially on the East Antarctic plateaus (e.g., the values of the topmost 1 cm of snow, the crystal ice in this study, can be up to >15 µeq L⁻¹; Fig. 1). Because of this, any comparison of NO₃⁻ concentrations in surface snow collected in different campaigns should be made with caution.

3.2 Snowpit NO₃⁻ concentrations

Mean NO₃⁻ concentrations for snowpits are shown in Fig. 1. From the coast to ~450 km inland, snowpit NO₃⁻ means are comparable to those of surface snow; whereas, NO₃⁻ means are lower in inland

snowpits than in surface snow with the exception of sites ~800 km from the coast. In general, the differences between snowpit NO_3^- means and the corresponding surface snow values are small at sites with high snow accumulation (e.g., close to coast), while the differences are large in low snow accumulation areas (e.g., near Dome A).

The profiles of NO_3^- for all snowpits are shown in Fig. 3. NO_3^- concentrations vary remarkably with depth in pits SP1 - SP5, which are located near the coast. Although SP2 and SP5 show high NO_3^- concentrations in the topmost sample, the data from deeper depths can be compared with the surface values. In addition, NO_3^- means for the entire snowpits are close to the means of the topmost layer covering a full annual cycle of accumulation (i.e., the most recent year of snow accumulation) at SP1-SP5 (Fig. 4). Given the high snow accumulation (Fig. 1), NO_3^- variability in coastal snowpits is likely suggestive of a seasonal signature (Wagenbach et al., 1998b; Grannas et al., 2007; Shi et al., 2015). Among the coastal snowpits, water isotope ratios ($\delta^{18}\text{O}$ of H_2O) of samples at SP2 were also determined, thus allowing for investigating NO_3^- seasonal variability (Fig. S3 in supporting information). In general, the $\delta^{18}\text{O}(\text{H}_2\text{O})$ peaks correspond to high NO_3^- concentrations (i.e., NO_3^- peaks present in summer). This seasonal pattern is in agreement with previous observations of NO_3^- in snow/ice and atmosphere in coastal Antarctica (Mulvaney and Wolff, 1993; Mulvaney et al., 1998; Wagenbach et al., 1998b; Savarino et al., 2007).

In contrast, most of the inland snowpits show high NO_3^- concentrations in the top layer, and then fall sharply from $> 2.0 \mu\text{eq L}^{-1}$ in top snow to $< 0.2 \mu\text{eq L}^{-1}$ in the first meter of depth (Fig. 3). NO_3^- means for the entire snowpits are typically lower than those of the most recent year snow layer (Fig. 4). Similar NO_3^- profiles for snowpits have been reported elsewhere in Antarctica, as a result of post-depositional processing of NO_3^- (R  hlisberger et al., 2000; McCabe et al., 2007; Erbland et al., 2013; Shi et al., 2015).

Comparison of the NO_3^- profile patterns reveals significant spatial heterogeneity, even for neighboring sites. For instance, sites SP11 and SP12, 14 km apart, feature similar snow accumulation rate (Table 1). If it is assumed that snow accumulation is relatively constant during the past several years at SP11 (sampled in 2012/2013), snow in the depth of ~54 cm corresponds to the deposition in 2009/2010 (snow density = 0.45 g cm^{-3} , from field measurements). NO_3^- concentrations are much higher in the top snow of SP12 (sampled in 2009/2010) than in the depth of ~54 cm in SP11 (Fig. 3). This variation in NO_3^- profiles at a local scale has been reported, possibly related to local morphologies associated with sastrugi formation and wind drift (Frey et al., 2009; Traversi et al., 2009). It is interesting that higher NO_3^- concentrations were not found in the uppermost layer at sites SP7 and SP8 (~600 km from coast; Fig. 3), where large sastrugi with hard smooth surfaces was extensively developed (from field observations; Fig. S4 in supporting information). Snow accumulation rate in this area fluctuates remarkably, and the values of some sites are rather small or close to zero due to the strong wind scouring (Fig. 1) (Ding et al., 2011; Das et al., 2013). In this case, the snowpit NO_3^- profiles appear to be largely influenced by wind scour on snow, possibly resulting in missing years and/or intra-annual mixing.

4 Discussion

4.1 Accumulation influence on NO_3^-

The preservation of NO_3^- is thought to be closely associated with snow accumulation, where most of the deposited NO_3^- is preserved at sites with higher snow accumulation (Wagenbach et al., 1994;

Hastings et al., 2004; Fibiger et al., 2013). Whereas NO_3^- may be altered significantly at sites with low snow accumulation, largely due to photolysis (Blunier et al., 2005; Grannas et al., 2007; Frey et al., 2009; Erbland et al., 2013; Erbland et al., 2015). In the following discussion, we divide the traverse into two zones, i.e., the coastal zone (<~450 km from the coast, including SP1-SP5 and Core 1; Table 1) and the inland region (~450 km to Dome A, including pits SP6-SP20 and Core 2; Table 1), following NO_3^- distribution patterns in surface snow and snowpits (sections 3.1 and 3.2) as well as the spatial pattern of snow accumulation rate (Fig. 1).

As for snowpits, NO_3^- levels in top and deeper layers are comparable near the coast, while NO_3^- differs considerably between the upper and deeper snow at inland sites (Figs. 3 and 4). Photochemical processing is responsible for NO_3^- distribution in inland snowpits (Erbland et al., 2013; Berhanu et al., 2015). Considering that the actinic flux is always negligible below the depth of 1 m, the bottom layers of the snowpits (i.e., > 100 cm; Table 1) are well below the photochemically active zone (France et al., 2011; Zatzko et al., 2013). In this case, NO_3^- in the bottom snowpit, i.e., below the photic zone, can be taken as the archived fraction without further modification, as also suggested by previous observations (Frey et al., 2009; Erbland et al., 2013; Erbland et al., 2015). Here, we define NO_3^- in the bottom layer covering a full annual cycle of deposition as an approximation of the annual mean of archived NO_3^- (i.e., beyond photochemical processing; denoted as “ C_{archived} ” in the following context; Fig. 4), thus allowing for calculating the archived annual NO_3^- flux (i.e., the product of C_{archived} and annual snow accumulation rate). Although there is uncertainty in the calculation of archived NO_3^- flux due to interannual variability in NO_3^- inputs and snow accumulation, this assumption provides a useful way to investigate the relationship between preservation of NO_3^- and physical factors considering that an extensive array of ice core measurements is unavailable in most of Antarctica. It is noted that C_{archived} is generally close to (lower than) the NO_3^- means for entire snowpits in coastal (inland) Antarctica (Fig. 4).

4.1.1 NO_3^- in coastal snowpack

The simplest plausible model to relate flux and concentration of NO_3^- in snow to its atmospheric concentration (Legrand, 1987; Alley et al., 1995) can be expressed as,

$$F_{\text{total}} = K_1 C_{\text{atm}} + K_2 C_{\text{atm}} A \quad (\text{Eq. 4}),$$

$$F_{\text{total}} = C_{\text{firn}} \times A \quad (\text{Eq. 5}),$$

where F_{total} is snow NO_3^- flux ($\mu\text{eq m}^{-2} \text{a}^{-1}$); C_{atm} is atmospheric concentration of NO_3^- ($\mu\text{eq m}^{-3}$); A is annual snow accumulation rate ($\text{kg m}^{-2} \text{a}^{-1}$); C_{firn} is measured firn NO_3^- concentration ($\mu\text{eq L}^{-1}$, here $C_{\text{firn}} = C_{\text{archived}}$); K_1 is the dry deposition velocity (cm s^{-1}); and K_2 is the scavenging ratio for precipitation ($\text{m}^3 \text{kg}^{-1}$), which allows conversion of atmospheric concentration to snow concentration of NO_3^- in this study. From Eqs. 4 and 5, firn NO_3^- concentration can be expressed as,

$$C_{\text{firn}} = K_1 C_{\text{atm}} \times 1/A + K_2 C_{\text{atm}} \quad (\text{Eq. 6})$$

If K_1 and K_2 are constants, a linear relationship between measured NO_3^- concentration (C_{firn}) and snow accumulation (A) can be interpreted using Eq. 6, which assumes regional spatial homogeneity of fresh snow NO_3^- levels and dry deposition flux. The slope ($K_1 C_{\text{atm}}$) of the linear model represents an approximation of dry deposition flux of NO_3^- (i.e., an apparent dry deposition flux), while the intercept ($K_2 C_{\text{atm}}$) stands for NO_3^- concentration in fresh snowfall. If dry deposition ($K_1 C_{\text{atm}}$) is much larger than wet deposition ($K_2 C_{\text{atm}} A$), the concentration of NO_3^- in snow will be proportional to its concentration in the atmosphere. In the condition of a constant atmospheric concentration, larger snow accumulation will increase the flux of NO_3^- but decrease its concentration in snow. While this linear model is a gross

over-simplification of the complex nature of air-snow exchange of NO_3^- , it provides a simple approach to compare the processes occurring on the coast versus those inland. In addition, this model can provide useful parameter values in modeling NO_3^- deposition/preservation at large scales, considering that observations remain sparse across Antarctica (e.g., Zatko et al., 2016).

The relationship between C_{archived} of NO_3^- and snow accumulation rate is shown in Fig. 5. The linear fit of C_{archived} vs. inverse snow accumulation ($R^2=0.88$, $p<0.01$; Fig. 5a) supports the assumptions of spatial homogeneity. The intercept and slope of the linear fit suggest a NO_3^- concentration in fresh snow and an apparent NO_3^- dry deposition flux of $0.7\pm0.07 \mu\text{eq L}^{-1}$ and $45.7\pm7.8 \mu\text{eq m}^{-2} \text{ a}^{-1}$ respectively. The apparent dry deposition flux is opposite to the observation in Dronning Maud Land (DML) region, where a negative dry deposition flux suggested net losses of NO_3^- (Pasteris et al., 2014).

Figure 5b shows the archived fluxes of NO_3^- on the coast, with values from 104 (at the lowest accumulation site) to $169 \mu\text{eq m}^{-2} \text{ a}^{-1}$ (at the highest accumulation site). Taking the calculated NO_3^- dry deposition flux of $45.7 \mu\text{eq m}^{-2} \text{ a}^{-1}$, dry deposition accounts for 27-44 % (mean = 36 %) of total NO_3^- inputs, with higher (lower) percentages at lower (higher) snow accumulation sites. This result is in line with the observations in Taylor Valley (coastal West Antarctica), where the snowfall was found to be the primary driver for NO_3^- inputs (Witherow et al., 2006). This observation also generally agrees with, but is greater than that in the modeling study of Zatko et al. (2016), which predicts a ratio of dry deposition to total deposition of NO_3^- in Antarctica as < 20 % close to the coast, increasing towards the plateaus.

In Figs. 5a and b, the strong linear relationships between NO_3^- and snow accumulation support that K_1 and K_2 are relatively constant on the coast (Eqs. 4 and 6). The average atmospheric concentration of NO_3^- in the coastal ~450 km region is 19.4 ng m^{-3} in summer (Table S1 in supporting information). Taking $C_{\text{atm}}=19.4 \text{ ng m}^{-3}$, K_1 is estimated to be 0.5 cm s^{-1} , identical to a typical estimate for HNO_3 deposition velocity to a snow/ice surface (0.5 cm s^{-1} ; Seinfeld and Pandis, 1997). This predicted K_1 value is lower than that calculated for the dry deposition of HNO_3 at South Pole (0.8 cm s^{-1} ; Huey et al., 2004). It is noted that the true K_1 value could be larger than the prediction (0.5 cm s^{-1}) due to the higher values of C_{atm} in summer (i.e., 19.4 ng m^{-3} for the calculation of K_1) than in other seasons (Mulvaney et al., 1998; Wagenbach et al., 1998b; Savarino et al., 2007). The scavenging ratio for precipitation (K_2) is calculated to be $0.2\times10^4 \text{ m}^3 \text{ kg}^{-1}$, i.e., $2 \text{ m}^3 \text{ g}^{-1}$.

If it is assumed that NO_3^- concentration in snow is related to its concentration in the atmosphere, the scavenging ratio for NO_3^- (W) can be calculated on a mass basis from the following expression (Kasper-Giebl et al., 1999),

$$W = \rho_{\text{atm}} \times (C_{\text{f-snow}} / C_{\text{atm}}) \text{ (Eq. 7),}$$

where ρ_{atm} is air density (g m^{-3}), and $C_{\text{f-snow}}$ and C_{atm} are NO_3^- concentrations in fresh snow (ng g^{-1}) and atmosphere (ng m^{-3}) respectively. If taking $\rho_{\text{atm}} \approx 1000 \text{ g m}^{-3}$ (on average, ground surface temperature $t \approx 255 \text{ K}$, ground pressure $P \approx 0.08 \text{ MPa}$, in the coastal region), $C_{\text{f-snow}} = 43 \text{ ng g}^{-1}$ (see discussion above and section 4.2 below), and $C_{\text{atm}} = 19.4 \text{ ng m}^{-3}$, W is calculated to be ~2200, generally comparable to previous reports (Barrie, 1985; Kasper-Giebl et al., 1999; Shrestha et al., 2002). It is noted that the calculation here may be subject to uncertainty, due to the complex transfer of atmospheric NO_3^- into the snow. However, the scavenging ratio provides valuable insights into the relation between NO_3^- concentrations in the atmosphere and snow, which might be useful in modeling NO_3^- deposition at a large-scale.

Figure 5c shows the distribution of flux is negatively correlated with C_{archived} of NO_3^- , which is not surprising since C_{archived} is positively related to inverse accumulation (Fig. 5a). Based on the observed

strong linear relationship between NO_3^- flux and snow accumulation (Fig. 5b), the archived NO_3^- flux is more accumulation dependent compared to C_{archived} . This is compatible with the observations in Greenland (Burkhart et al., 2009), where accumulation is generally above $100 \text{ kg m}^{-2} \text{ a}^{-1}$, similar to the coastal values in this study.

In terms of surface snow on the coast, NO_3^- may be disturbed by the katabatic winds and wind convergence located near the Amery Ice Shelf (that is, the snow-sourced NO_x and NO_3^- from the Antarctic plateau possibly contributes to coastal snow NO_3^-) (Parish and Bromwich, 2007; Ma et al., 2010; Zatko et al., 2016). In addition, the sampled $\sim 3 \text{ cm}$ surface layer roughly corresponds to the net accumulation in the past 0.5-1.5 months assuming an even distribution of snow accumulation in the course of a single year. This difference in exposure time of the surface snow at different sampling sites, could possibly affect the concentration of NO_3^- , although the post-depositional alteration of NO_3^- was thought to be minor on the coast (Wolff et al., 2008; Erbland et al., 2013; Shi et al., 2015). Taken together, NO_3^- in coastal surface snow might represent some post-depositional alteration. Even so, a negative correlation between NO_3^- concentration and snow accumulation rate was found at the coast ($R^2=0.42$, $p<0.01$; Fig. 6a), suggesting that overall the majority of the NO_3^- appears to be preserved and is determined by snow accumulation.

4.1.2 NO_3^- in inland snowpack

In comparison with the coast, the correlation between C_{archived} and inverse snow accumulation is relatively weak in inland regions (Fig. 5d), suggesting more variable conditions in ambient concentrations and dry deposition flux of NO_3^- . In addition, the relationship of C_{archived} vs. inverse accumulation inland is opposite to that of coast. Based on current understanding of the post-depositional processing of NO_3^- , the negative correlation between C_{archived} and inverse snow accumulation (Fig. 5d) suggests losses of NO_3^- . The slope of the linear relationship indicates apparent NO_3^- dry deposition flux of $-44.5 \pm 13.0 \text{ } \mu\text{eq m}^{-2} \text{ a}^{-1}$, much larger than that of DML ($-22.0 \pm 2.8 \text{ } \mu\text{eq m}^{-2} \text{ a}^{-1}$), where the snow accumulation is generally lower than $100 \text{ kg m}^{-2} \text{ a}^{-1}$ (Pasteris et al., 2014). At Kohnen Station (an inland site in East Antarctica), with snow accumulation of $71 \text{ kg m}^{-2} \text{ a}^{-1}$, the emission flux of NO_3^- is estimated to be $-22.9 \pm 3.7 \text{ } \mu\text{eq m}^{-2} \text{ a}^{-1}$ (Weller and Wagenbach, 2007), which is also smaller in comparison with this observation. Weller et al. (2004) proposed that loss rate of NO_3^- does not depend on snow accumulation rate and the losses become insignificant at accumulation rates above $100 \text{ kg m}^{-2} \text{ a}^{-1}$. Among the inland sites, SP10 and Core2 ($\sim 800 \text{ km}$ from the coast), featured by high snow accumulation rate ($> 100 \text{ kg m}^{-2} \text{ a}^{-1}$; Table 1 and Fig. 1), exhibit even higher values of C_{archived} and archived fluxes of NO_3^- than those of the coastal sites. It is noted that these two cases influence the linear regression significantly (Fig. 5d). If the two sites are excluded, we can get a linear regression with a slope of $-27.7 \pm 9.2 \text{ } \mu\text{eq m}^{-2} \text{ a}^{-1}$, which is comparable to previous reports in DML (Pasteris et al., 2014).

The depths of inland snowpits cover several to tens of years snow accumulation, thus allowing for directly investigating NO_3^- emission rate. The difference between NO_3^- concentrations in the snow layer accumulated during the most recent year (Fig. 4) and in the snow accumulated during the year before the most recent year can represent the loss rate of NO_3^- . If it is assumed that snow accumulation rate is relatively constant during recent decades at specific-sites, on average, $36.7 \pm 21.3 \%$ of NO_3^- (in $\mu\text{eq L}^{-1}$) was lost during one year, with the two sites (SP10 and Core2) with snow accumulation $> 100 \text{ kg m}^{-2} \text{ a}^{-1}$ excluded from the calculation. The percentages are generally higher at the sites with lower snow accumulation rate. Together with snow accumulation rate, the emission flux of NO_3^- is calculated

to be $-28.1 \pm 23.0 \mu\text{eq m}^{-2} \text{ a}^{-1}$, close to the linear model prediction ($-27.7 \pm 9.2 \mu\text{eq m}^{-2} \text{ a}^{-1}$). Significant losses can account for NO_3^- profiles at inland sites, i.e., NO_3^- concentration decreasing with increasing depths. Previous observations and modeling works suggested that photolysis dominates the losses (Frey et al., 2009; Erbland et al., 2013; Shi et al., 2015). During photolysis of NO_3^- , some of the photoproducts (NO_x) are emitted into the gas phase (Davis et al., 2004; France et al., 2011), and these products should undergo reoxidation by the local oxidants (e.g., hydroxyl radical (OH), $\text{NO}_2 + \text{OH} + \text{M} \rightarrow \text{HNO}_3 + \text{M}$), forming gas phase HNO_3 . In inland Antarctica, the dominant NO_3^- species in the atmosphere is gaseous HNO_3 during summertime, while particulate NO_3^- is more important in winter (Legrand et al., 2017b; Traversi et al., 2017). The high levels of gas phase HNO_3 in summer support the importance of the re-emission from snow through the photolysis of NO_3^- in affecting the atmospheric $\text{NO}_x/\text{NO}_3^-$ budget (Erbland et al., 2013). On the one hand, the gaseous HNO_3 can be efficiently co-condensed with water vapour onto the extensively developed crystal ice layers on Antarctic plateaus (e.g., Fig. S1 in supporting information), leading to an enrichment of NO_3^- in surface snow (Bock et al., 2016). On the other hand, a large concentration of HNO_3 would enhance its reaction with sea-salt, leading to elevated particulate NO_3^- concentrations (Legrand et al., 2017b). The significant correlation between NO_3^- and H^+ in inland Antarctic surface snow ($R^2 = 0.65$, $p < 0.01$) seems to support the importance of atmospheric gas phase HNO_3 in affecting surface snow NO_3^- concentrations, in particular NO_3^- levels in the crystal ice samples (Fig. 1).

Several modeling works have been performed to understand NO_3^- recycling processes across Antarctica (e.g., Erbland et al., 2015; Zatko et al., 2016; Bock et al., 2016), however, each employs different assumptions and large uncertainty remains in quantifying NO_3^- recycling and preservation. It is thought that emission and transport strength are the main factors controlling the recycling of NO_3^- , while the former is associated with initial NO_3^- concentrations, UV and snow optical properties, and the latter is linked with air mass movement (Wolff et al., 2008; Frey et al., 2009). As a result, snow accumulation alone is likely insufficient to account for NO_3^- variability in surface snow (i.e., no significant correlation between NO_3^- concentration and snow accumulation; Fig. 6b).

The archived NO_3^- fluxes vary considerably among inland sites, from ~ 3 to $333 \mu\text{eq m}^{-2} \text{ a}^{-1}$, with high values generally corresponding to high snow accumulation (Fig. 5e). However, the nearly 1:1 relationship between C_{archived} and NO_3^- flux (Fig. 5f), suggests that accumulation rate is not the main driver of the archived NO_3^- concentration. In inland Antarctica, the archived NO_3^- fraction is largely influenced by the length of time that NO_3^- was exposed to UV radiation (Berhanu et al., 2015), which decreases exponentially in the snowpack. The e -folding depth, z_e value, is thought to be influenced by a variety of factors, such as co-existent impurities (e.g., black carbon), bulk density and grain size (Zatko et al., 2013). In addition, the snow albedo is also dependent on snow physical properties (Carmagnola et al., 2013). Taken together, this suggests that the inland plateau is below a “threshold” of accumulation rate such that the archived NO_3^- flux cannot be explained by snow accumulation rate.

4.2 Effects of coexisting ions on NO_3^-

Atmospheric NO_3^- in Antarctica is thought to be mainly associated with mid-latitude sources, re-formed NO_3^- driven by snow-sourced photolysis products, and/or stratospheric inputs (Savarino et al., 2007; Lee et al., 2014; Traversi et al., 2017 and references therein). Although organic nitrates can play an important role in the atmospheric NO_y budget, multi-seasonal measurements of surface snow NO_3^- correlate strongly with inorganic NO_y species (especially HNO_3) rather than organic (Jones et al., 2011). Here, we investigate whether NO_3^- in snow is closely associated with coexisting ions (e.g., Cl^- ,

SO₄²⁻, Na⁺, K⁺, Mg²⁺ and Ca²⁺) since these ions have different main sources, e.g., Cl⁻ and Na⁺ are predominantly influenced by sea salt, and SO₄²⁻ is likely dominated by marine inputs (e.g., sea salt and bio-activity source) (Bertler et al., 2005). In the snow, Cl⁻, Na⁺ and SO₄²⁻ are the most abundant ions in addition to NO₃⁻.

In surface snow, the non-sea salt fraction of SO₄²⁻ accounted for 75-99 % of its total budget, with a mean of 95 %. The percentages were relatively higher in inland regions than at coastal sites. On the coast, a positive relationship was found between nssSO₄²⁻ and NO₃⁻ ($R^2 = 0.32$, $p < 0.01$; Fig. 7a). Previous observations suggest that NO₃⁻ and nssSO₄²⁻ peaks in the atmosphere and snow are usually present in summer (Jourdain and Legrand, 2002; Wolff et al., 2008; Sigl et al., 2016; Legrand et al., 2017a; Legrand et al., 2017b). However, the similar seasonal pattern of the two species is associated with distinct sources, i.e., SO₄²⁻ is mainly derived from marine biogenic emissions while NO₃⁻ is influenced by photolysis and tropospheric transport (Savarino et al., 2007; Lee et al., 2014; Zatko et al., 2016). In the atmosphere, SO₄²⁻ is typically found on the submicron particles, while most of the NO₃⁻ is gaseous HNO₃ and the particulate NO₃⁻ is mainly on intermediate size particles (Jourdain and Legrand, 2002; Rankin and Wolff, 2003; Legrand et al., 2017a; Legrand et al., 2017b). Thus, the correlation between NO₃⁻ and SO₄²⁻ is unlikely explained by the sources or their occurrence state in the atmosphere (i.e., gaseous and particulate phases). Laluraj et al. (2010) proposed that the correlation between nssSO₄²⁻ vs. NO₃⁻ in ice ($R^2 = 0.31$, $p < 0.01$) could be associated with fine nssSO₄²⁻ aerosols, which provide nucleation centers forming multi-ion complexes with HNO₃ in the atmosphere. This assertion, however, should be examined further, considering that the complex chemistry of SO₄²⁻ and NO₃⁻ in the atmosphere is far from understood (e.g., Wolff, 1995; Brown et al., 2006). Thus far, the mechanism of nssSO₄²⁻ influencing NO₃⁻ in the snowpack, however, is still debated, and it cannot be ruled out that nssSO₄²⁻ further affects mobilization of NO₃⁻ during and/or after crystallization (Legrand and Kirchner, 1990; Wolff, 1995; R  hlisberger et al., 2000). It is noted that no relationship was found between nssSO₄²⁻ and NO₃⁻ in inland snow (Fig. 7d), possibly due to the strong alteration of NO₃⁻ during post-depositional processes, as discussed in section 4.1.2.

In comparison with nssSO₄²⁻ aerosols, the sea-salt aerosols (Na⁺) are coarser and can be removed preferentially from the atmosphere due to a larger dry deposition velocity. High atmospheric sea salt aerosol concentrations are expected to promote the conversion of gaseous HNO₃ to the particulate phase, considering that most of the NO₃⁻ in the atmosphere is in the gas phase (HNO₃). In this case, particulate NO₃⁻ can be efficiently lost via aerosol mechanisms. In addition, the saline ice also favors the direct uptake of gaseous HNO₃ to the ice surface. Changes in partitioning between gas phase (HNO₃) and particulate phase will affect NO₃⁻ levels due to the different wet and dry deposition rates of the two species (Aw and Kleeman, 2003). Thus, sea salt aerosols play an important role in the scavenging of gaseous HNO₃ from the atmosphere (Hara et al., 2005), and elevated NO₃⁻ concentrations are usually accompanied by Na⁺ spikes in the snowpack (e.g., at Halley station; Wolff et al., 2008). Surprisingly, no significant correlation was found between Na⁺ and NO₃⁻ in coastal snow (Fig. 7b). The concentration profiles of NO₃⁻ and Na⁺ in coastal surface snow are shown in Fig. 8, and NO₃⁻ roughly corresponds to Na⁺ in some areas, e.g., 50-150 km and 300-450 km distance inland, although in general they are not very coherent. It is noted that amongst the 4 snow samples with Na⁺ > 1.5 µeq L⁻¹ (open circles in Fig. 8), only one sample co-exhibits a NO₃⁻ spike. This is different from observations at Halley station, where Na⁺ peaks usually led to elevated NO₃⁻ levels in surface snow in summer (Wolff et al., 2008). Of the 4 largest Na⁺ spikes, one is a fresh snowfall sample (dashed ellipse in Fig. 8), and this sample shows the highest Na⁺ concentration (2.8 µeq L⁻¹) and low NO₃⁻ (0.75 µeq

L⁻¹). It is noted that NO₃⁻ concentration in this fresh snowfall is close to the model predictions (0.7±0.07 µeq L⁻¹; section 4.1.1), validating that the simple linear deposition model (i.e., the Eq. 6) can well depict the deposition and preservation of NO₃⁻ in coastal snowpack. At inland sites, no correlation was found between NO₃⁻ and Na⁺ (Fig. 7e), likely explained by the alteration of NO₃⁻ concentration by post-depositional processing.

In surface snow, nssCl⁻ represents 0-64 % (mean = 40 %) of the total Cl⁻. On the coast, it is of interest that nssCl⁻ in the 4 samples with the highest Na⁺ concentrations (open circles in Figs. 7b and 8) are close to 0, and positive nssCl⁻ values were found for the other samples. The fractionation of Na⁺ can occur due to mirabilite precipitation in sea-ice formation at <-8 °C (Marion et al., 1999), possibly leading to the positive nssCl⁻. However, even if all of SO₄²⁻ in sea water is removed via mirabilite precipitation, only 12 % of sea salt Na⁺ is lost (Rankin et al., 2002). Considering the smallest sea ice extent in summertime in East Antarctica (Holland et al., 2014), the high Cl⁻/Na⁺ ratio (mean = 2.1, well above 1.17 of sea water, in µeq L⁻¹) in surface snow is unlikely from sea salt fractionation associated with mirabilite precipitation in sea-ice formation. In this case, nssCl⁻ could be mainly related to the deposition of volatile HCl, which is from the reaction of H₂SO₄ and/or HNO₃ with NaCl (Röhrlisberger et al., 2003). Thus, nssCl⁻ in snowpack can roughly represent the atmospherically deposited HCl. In summertime, most of the dechlorination (i.e., production of HCl) is likely associated with HNO₃ due to its high atmospheric concentrations (Jourdain and Legrand, 2002; Legrand et al., 2017b). Accordingly, the observed relationship between NO₃⁻ and nssCl⁻ (Fig. 7c) appears to suggest that HCl production can be enhanced by elevated HNO₃ levels in the atmosphere.

With regard to the crystal ice, no significant correlation was found between NO₃⁻ and the coexisting ions (e.g., Cl⁻, Na⁺ and SO₄²⁻), suggesting that these ions are generally less influential on NO₃⁻ in this uppermost thin layer, compared to the strong air-snow transfer process of NO₃⁻ (Erbland et al., 2013). It is noted that NO₃⁻ accounts for most of the calculated H⁺ concentrations (81-97 %, mean = 89 %), and a strong linear relationship was found between them ($R^2 = 0.96$, $p < 0.01$), suggesting that NO₃⁻ is mainly deposited as acid, HNO₃, rather than in particulate form as salts (e.g., NaNO₃ and Ca(NO₃)₂). This deduction is in line with the atmospheric observations at Dome C, where NO₃⁻ was found to be mainly in gaseous phase (HNO₃) in summer (Legrand et al., 2017b). On average, the deposition of HNO₃ contributes > 91 % of NO₃⁻ in the crystal ice (the lower limit, 91 %, calculated by assuming all of the alkaline species (Na⁺, NH₄⁺, K⁺, Mg²⁺ and Ca²⁺) are neutralized by HNO₃ in the atmosphere), suggesting a dominant role of HNO₃ deposition in snow NO₃⁻ concentrations. The elevated high atmospheric NO₃⁻ concentrations observed at Dome A (>100 ng m⁻³; 77.12°E and 80.42°S, Table S1 in supporting information) possibly indicate oxidation of gaseous NO_x to HNO₃, providing further evidence that NO₃⁻ recycling driven by photolysis plays an important role in its abundance in snowpack on East Antarctic plateaus.

5 Conclusions

Samples of surface snow, snowpits and the uppermost layer of crystal ice, collected on the traverse from the coast to Dome A, East Antarctica, were used to investigate the deposition and preservation of NO₃⁻ in snow. In general, a spatial trend of NO₃⁻ in surface snow was found on the traverse, with high (low) concentrations on the plateau (coast). Similarly, NO₃⁻ concentrations in the atmosphere are higher on the plateau than at coastal sites, with a range of 8 to 183 ng m⁻³. Extremely high NO₃⁻ levels (e.g., > 10 µeq L⁻¹) were observed in the uppermost crystal ice layer, possibly associated with re-deposition of recycled NO₃⁻ from snow-sourced NO_x. As for the snowpits, NO₃⁻ exhibits high levels in the top layer

and low concentrations at deeper depths in the inland region, while no clear trend was found on the coast.

On the coast, the archived NO_3^- flux in snow is positively correlated with snow accumulation rate, but negatively with NO_3^- concentration. A linear model can well depict the relationship between archived NO_3^- and snow accumulation, supporting that atmospheric levels and dry deposition fluxes of NO_3^- are spatially homogeneous on the coast, and that dry deposition plays a minor role in snow NO_3^- inputs. The dry deposition velocity and scavenging ratio for NO_3^- are estimated to be 0.5 cm s^{-1} and 2200, respectively. In inland Antarctica, the archived NO_3^- fluxes, varying significantly among sites, are largely dependent on NO_3^- concentration. A weak correlation between snow accumulation and archived NO_3^- suggests variable ambient concentrations and dry deposition flux of NO_3^- , and the relationship is opposite to that for the coast. This supports the idea that post-depositional processing dominates NO_3^- concentration and distribution in inland Antarctica (e.g., Erbland et al., 2013; Erbland et al., 2015; Shi et al., 2015; Zatko et al., 2016).

The major ions, Cl^- , SO_4^{2-} and Na^+ , originate from different sources than NO_3^- , but could potentially affect the scavenging and preservation of NO_3^- . In coastal surface snow, a positive correlation between SO_4^{2-} and NO_3^- suggests the potential influence of fine aerosols on NO_3^- formation and/or scavenging, while the coarse sea salt aerosol (e.g., Na^+) is likely less influential. In contrast to the coast, NO_3^- in inland surface snow is dominated by post-depositional processes, and the effects of coexisting ions on NO_3^- appear to be rather minor. In inland surface snow, the strong relationship between NO_3^- and H^+ suggests a dominant role of gaseous HNO_3 deposition in determining NO_3^- concentrations.

Associated content

Please see the file of Supporting Information.

Data availability

Data on nitrate concentrations in snow and atmosphere on the traverse from coast (Zhongshan Station) to Dome A can be made available for scientific purposes upon request to the author, G.S. (contact: gt_shi@163.com).

Competing interests

The authors declare that they have no conflict of interest.

Acknowledgement

This project was supported by the National Science Foundation of China (Grant nos. 41576190 and 41206188 to GS, 41476169 to SJ), the National Key Research and Development Program of China (Grant no. 2016YFA0302204), the Fundamental Research Funds for the Central Universities (Grant No 40500-20101-222006), and Chinese Polar Environment Comprehensive Investigation and Assessment Programmes (Grant nos. CHINARE 201X-02-02 and 201X-04-01). The authors appreciate the CHINARE inland members for providing help during sampling. The authors would like to thank Prof. Joel Savarino and two anonymous referees for their help in the development and improvement of this paper.

References

Alexander, B., Savarino, J., Kreutz, K.J., and Thiemens, M.: Impact of preindustrial biomass-burning

emissions on the oxidation pathways of tropospheric sulfur and nitrogen, *J. Geophys. Res.*, 109, D08303, doi:10.1029/2003JD004218, 2004.

Alley, R., Finkel, R., Nishizumi, K., Anandakrishnan, A., Shuman, C., Mershon, G., Zielinski, G., and Mayewski, P.A.: Changes in continental and sea-salt atmospheric loadings in central Greenland during the most recent deglaciation: Model-based estimates, *J. Glaciol.*, 41, 503-514, 1995.

Arthern, R.J., Winebrenner, D.P., and Vaughan, D.G.: Antarctic snow accumulation mapped using polarization of 4.3-cm wavelength microwave emission, *J. Geophys. Res.*, 111, doi:10.1029/2004JD005667, 2006.

Aw, J., and Kleeman, M.J.: Evaluating the first-order effect of intraannual temperature variability on urban air pollution, *J. Geophys. Res.*, 108, -, 2003.

Barrie, L.A.: Scavenging ratios, wet deposition, and in-cloud oxidation: An application to the oxides of sulphur and nitrogen, *J. Geophys. Res.*, 90, 5789-5799, 1985.

Berhanu, T.A., Meusinger, C., Erbland, J., Jost, R., Bhattacharya, S., Johnson, M.S., and Savarino, J.: Laboratory study of nitrate photolysis in Antarctic snow. II. Isotopic effects and wavelength dependence, *J. Chem. Phys.*, 140, 244306, doi:10.1063/1.4882899, 2014.

Berhanu, T.A., Savarino, J., Erbland, J., Vicars, W.C., Preunkert, S., Martins, J.F., and Johnson, M.S.: Isotopic effects of nitrate photochemistry in snow: a field study at Dome C, Antarctica, *Atmos. Chem. Phys.*, 15, 11243-11256, doi:10.5194/acp-15-11243-2015, 2015.

Bertler, N., Mayewski, P.A., Aristarain, A., Barrett, P., Becagli, S., Bernardo, R., Bo, S., Xiao, C., Curran, M., and Qin, D.: Snow chemistry across Antarctica, *Ann. Glaciol.*, 41, 167-179, 2005.

Blunier, T., Floch, G., Jacoby, H.-W., and Quansah, E.: Isotopic view on nitrate loss in Antarctic surface snow, *Geophys. Res. Lett.*, 32, L13501, doi:10.1029/2005GL023011, 2005.

Bock, J., Savarino, J., and Picard, G.: Air-snow exchange of nitrate: a modelling approach to investigate physicochemical processes in surface snow at Dome C, Antarctica, *Atmos. Chem. Phys.*, 16, 12531-12550, doi:10.5194/acp-16-12531-2016, 2016.

Brown, S., Ryerson, T., Wollny, A., Brock, C., Peltier, R., Sullivan, A., Weber, R., Dube, W., Trainer, M., and Meagher, J.: Variability in nocturnal nitrogen oxide processing and its role in regional air quality, *Science*, 311, 67-70, doi:10.1126/science.1120120, 2006.

Burkhart, J.F., Bales, R.C., McConnell, J.R., Hutterli, M.A., and Frey, M.M.: Geographic variability of nitrate deposition and preservation over the Greenland Ice Sheet, *J. Geophys. Res.*, 114, doi:10.1029/2008JD010600, 2009.

Carmagnola, C., Domine, F., Dumont, M., Wright, P., Strellis, B., Bergin, M., Dibb, J., Picard, G., and Morin, S.: Snow spectral albedo at Summit, Greenland: measurements and numerical simulations based on physical and chemical properties of the snowpack, *The Cryosphere*, 7, 1139-1160, doi:10.5194/tc-7-1139-2013, 2013.

Das, I., Bell, R.E., Scambos, T.A., Wolovick, M., Creyts, T.T., Studinger, M., Frearson, N., Nicolas, J.P., Lenaerts, J.T., and van den Broeke, M.R.: Influence of persistent wind scour on the surface mass balance of Antarctica, *Nat. Geosci.*, 6, 367-371, doi:10.1038/NGEO1766, 2013.

Davis, D., Chen, G., Buhr, M., Crawford, J., Lenschow, D., Lefer, B., Shetter, R., Eisele, F., Mauldin, L., and Hogan, A.: South Pole NO_x chemistry: an assessment of factors controlling variability and absolute levels, *Atmos. Environ.*, 38, 5375-5388, doi:10.1016/j.atmosenv.2004.04.039, 2004.

Dibb, J.E., Gregory Huey, L., Slusher, D.L., and Tanner, D.J.: Soluble reactive nitrogen oxides at South Pole during ISCAT 2000, *Atmos. Environ.*, 38, 5399-5409, doi:10.1016/j.atmosenv.2003.01.001, 2004.

Ding, M., Xiao, C., Jin, B., Ren, J., Qin, D., and Sun, W.: Distribution of $\delta^{18}\text{O}$ in surface snow along a

transect from Zhongshan Station to Dome A, East Antarctica, *Chin. Sci. Bull.*, 55, 2709-2714, doi:10.1007/s11434-010-3179-3, 2010.

Ding, M., Xiao, C., Li, Y., Ren, J., Hou, S., Jin, B., and Sun, B.: Spatial variability of surface mass balance along a traverse route from Zhongshan station to Dome A, Antarctica, *J. Glaciol.*, 57, 658-666, 2011.

Duderstadt, K.A., Dibb, J.E., Jackman, C.H., Randall, C.E., Solomon, S.C., Mills, M.J., Schwadron, N.A., and Spence, H.E.: Nitrate deposition to surface snow at Summit, Greenland, following the 9 November 2000 solar proton event, *J. Geophys. Res.*, 119, 6938-6957, 2014.

Duderstadt, K.A., Dibb, J.E., Schwadron, N.A., Spence, H.E., Solomon, S.C., Yudin, V.A., Jackman, C.H., and Randall, C.E.: Nitrate ion spikes in ice cores not suitable as proxies for solar proton events, *J. Geophys. Res.*, 121, 2994-3016, doi:10.1002/2015JD023805, 2016.

Erbland, J., Savarino, J., Morin, S., France, J.L., Frey, M.M., and King, M.D.: Air-snow transfer of nitrate on the East Antarctic plateau -Part 2: An isotopic model for the interpretation of deep ice-core records, *Atmos. Chem. Phys.*, 15, 12079-12113, doi:10.5194/acp-15-12079-2015, 2015.

Erbland, J., Vicars, W., Savarino, J., Morin, S., Frey, M., Frosini, D., Vince, E., and Martins, J.: Air-snow transfer of nitrate on the East Antarctic Plateau - Part 1: Isotopic evidence for a photolytically driven dynamic equilibrium in summer, *Atmos. Chem. Phys.*, 13, 6403-6419, doi:10.5194/acp-13-6403-2013, 2013.

Felix, J.D., and Elliott, E.M.: The agricultural history of human - nitrogen interactions as recorded in ice core $\delta^{15}\text{N}$ - NO_3^- , *Geophys. Res. Lett.*, 40, 1642-1646, doi:10.1002/grl.50209, 2013.

Fibiger, D.L., Hastings, M.G., Dibb, J.E., and Huey, L.G.: The preservation of atmospheric nitrate in snow at Summit, Greenland, *Geophys. Res. Lett.*, 40, 3484-3489, doi:10.1002/grl.50659, 2013.

France, J., King, M., Frey, M., Erbland, J., Picard, G., Preunkert, S., MacArthur, A., and Savarino, J.: Snow optical properties at Dome C (Concordia), Antarctica; implications for snow emissions and snow chemistry of reactive nitrogen, *Atmos. Chem. Phys.*, 11, 9787-9801, doi:10.5194/acp-11-9787-2011, 2011.

Frey, M.M., Savarino, J., Morin, S., Erbland, J., and Martins, J.: Photolysis imprint in the nitrate stable isotope signal in snow and atmosphere of East Antarctica and implications for reactive nitrogen cycling, *Atmos. Chem. Phys.*, 9, 8681-8696, 2009.

Geng, L., Alexander, B., Cole-Dai, J., Steig, E.J., Savarino, J., Sofen, E.D., and Schauer, A.J.: Nitrogen isotopes in ice core nitrate linked to anthropogenic atmospheric acidity change, *Proc. Natl. Acad. Sci.*, 111, 5808-5812, doi:10.1073/pnas.1319441111, 2014.

Geng, L., Murray, L.T., Mickley, L.J., Lin, P., Fu, Q., Schauer, A.J., and Alexander, B.: Isotopic evidence of multiple controls on atmospheric oxidants over climate transitions, *Nature*, 546, 133-136, doi:10.1038/nature22340, 2017.

Goodwin, I., De Angelis, M., Pook, M., and Young, N.: Snow accumulation variability in Wilkes Land, East Antarctica, and the relationship to atmospheric ridging in the 130° - 170° E region since 1930, *J. Geophys. Res.*, 108, doi:10.1029/2002JD002995, 2003.

Grannas, A., Jones, A.E., Dibb, J., Ammann, M., Anastasio, C., Beine, H., Bergin, M., Bottenheim, J., Boxe, C., and Carver, G.: An overview of snow photochemistry: evidence, mechanisms and impacts, *Atmos. Chem. Phys.*, 7, 4329-4373, 2007.

Hara, K., Osada, K., Kido, M., Matsunaga, K., Iwasaka, Y., Hashida, G., and Yamanouchi, T.: Variations of constituents of individual sea-salt particles at Syowa station, Antarctica, *Tellus B*, 57, 230-246, 2005.

Hastings, M.G., Jarvis, J.C., and Steig, E.J.: Anthropogenic impacts on nitrogen isotopes of ice-core nitrate, *Science*, 324, 1288-1288, doi:10.1126/science.1170510, 2009.

750 Hastings, M.G., Steig, E., and Sigman, D.: Seasonal variations in N and O isotopes of nitrate in snow at
751 Summit, Greenland: Implications for the study of nitrate in snow and ice cores, *J. Geophys. Res.*, 109,
752 D20306, doi:10.1029/2004JD004991, 2004.

753 Holland, P.R., Bruneau, N., Enright, C., Losch, M., Kurtz, N.T., and Kwok, R.: Modeled Trends in Antarctic
754 Sea Ice Thickness, *J. Climate*, 27, 3784-3801, doi:10.1175/JCLI-D-13-00301.1, 2014.

755 Hou, S., Li, Y., Xiao, C., and Ren, J.: Recent accumulation rate at Dome A, Antarctica, *Chin. Sci. Bull.*, 52,
756 428-431, 2007.

757 Huey, L.G., Tanner, D.J., Slusher, D.L., Dibb, J.E., Arimoto, R., Chen, G., Davis, D., Buhr, M.P., Nowak, J.B.,
758 Mauldin Iii, R.L., Eisele, F.L., and Kosciuch, E.: CIMS measurements of HNO₃ and SO₂ at the South Pole
759 during ISCAT 2000, *Atmos. Environ.*, 38, 5411-5421, doi:10.1016/j.atmosenv.2004.04.037, 2004.

760 Jones, A.E., Weller, R., Minikin, A., Wolff, E.W., Sturges, W.T., McIntyre, H.P., Leonard, S.R., Schrems, O.,
761 and Bauguitte, S.: Oxidized nitrogen chemistry and speciation in the Antarctic troposphere, *J. Geophys.*
762 *Res.*, 1042, 21355-21366, 1999.

763 Jones, A.E., Wolff, E.W., Ames, D., Bauguitte, S.-B., Clemitshaw, K., Fleming, Z., Mills, G., Saiz-Lopez, A.,
764 Salmon, R.A., and Sturges, W.: The multi-seasonal NO_y budget in coastal Antarctica and its link with
765 surface snow and ice core nitrate: results from the CHABLIS campaign, *Atmos. Chem. Phys.*, 11,
766 9271-9285, 2011.

767 Jourdain, B., and Legrand, M.: Year - round records of bulk and size - segregated aerosol composition
768 and HCl and HNO₃ levels in the Dumont d'Urville (coastal Antarctica) atmosphere: Implications for
769 sea - salt aerosol fractionation in the winter and summer, *J. Geophys. Res.*, 107, ACH 20-21 – ACH
770 20-13, doi:10.1029/2002JD002471, 2002.

771 Kasper-Giebl, A., Kalina, M.F., and Puxbaum, H.: Scavenging ratios for sulfate, ammonium and nitrate
772 determined at Mt. Sonnblick (3106m a.s.l.), *Atmos. Environ.*, 33, 895-906, 1999.

773 Laluraj, C., Thamban, M., Naik, S., Redkar, B., Chaturvedi, A., and Ravindra, R.: Nitrate records of a
774 shallow ice core from East Antarctica: Atmospheric processes, preservation and climatic implications,
775 *The Holocene*, 21, 351-356, doi:10.1177/0959683610374886, 2010.

776 Lee, H.-M., Henze, D.K., Alexander, B., and Murray, L.T.: Investigating the sensitivity of surface-level
777 nitrate seasonality in Antarctica to primary sources using a global model, *Atmos. Environ.*, 89, 757-767,
778 doi:10.1016/j.atmosenv.2014.03.003, 2014.

779 Legrand, M.: Chemistry of Antarctic snow and ice, *Le Journal De Physique Colloques*, 48, C1-77-C71-86,
780 1987.

781 Legrand, M., and Kirchner, S.: Origins and variations of nitrate in South Polar precipitation, *J. Geophys.*
782 *Res.*, 95, 3493-3507 1990.

783 Legrand, M., and Mayewski, P.A.: Glaciochemistry of polar ice cores: a review, *Rev. Geophys.*, 35,
784 219-243, 1997.

785 Legrand, M., Preunkert, S., Weller, R., Zipf, L., Elsässer, C., Merchel, S., Rugel, G., and Wagenbach, D.:
786 Year-round record of bulk and size-segregated aerosol composition in central Antarctica (Concordia
787 site) – Part 2: Biogenic sulfur (sulfate and methanesulfonate) aerosol, *Atmos. Chem. Phys.*, 17,
788 14055-14073, doi:10.5194/acp-17-14055-2017, 2017a.

789 Legrand, M., Preunkert, S., Wolff, E., Weller, R., Jourdain, B., and Wagenbach, D.: Year-round records of
790 bulk and size-segregated aerosol composition in central Antarctica (Concordia site) – Part 1:
791 Fractionation of sea-salt particles, *Atmos. Chem. Phys.*, 17, 14039-14054,
792 doi:10.5194/acp-17-14039-2017, 2017b.

793 Legrand, M., Wolff, E., and Wagenbach, D.: Antarctic aerosol and snowfall chemistry: implications for

794 deep Antarctic ice-core chemistry, *Ann. Glaciol.*, 29, 66-72, 1999.
 795 Legrand, M.R., Stordal, F., Isaksen, I.S.A., and Rognnerud, B.: A model study of the stratospheric budget
 796 of odd nitrogen, including effects of solar cycle variations, *Tellus Series B-chemical & Physical*
 797 *Meteorology*, 41B, 413–426, doi:10.1111/j.1600- 0889.1989.tb00318.x, 1989.
 798 Li, C., Ren, J., Qin, D., Xiao, C., Hou, S., Li, Y., and Ding, M.: Factors controlling the nitrate in the DT-401
 799 ice core in eastern Antarctica, *Sci. China Ser. D*, doi:10.1007/s11430-012-4557-2, 2013.
 800 Li, Y., Cole-Dai, J., and Zhou, L.: Glaciochemical evidence in an East Antarctica ice core of a recent (AD
 801 1450-1850) neoglacial episode, *J. Geophys. Res.*, 114, doi:10.1029/2008JD011091, 2009.
 802 Li, Z., Zhang, M., Qin, D., Xiao, C., Tian, L., Kang, J., and Li, J.: The seasonal variations of $\delta^{18}\text{O}$, Cl^- , Na^+ ,
 803 NO_3^- and Ca^{2+} in the snow and firn recovered from Princess Elizabeth Land, Antarctica, *Chin. Sci. Bull.*,
 804 44, 2270-2273, 1999.
 805 Liss, P.S., Chuck, A.L., Turner, S.M., and Watson, A.J.: Air-sea gas exchange in Antarctic waters, *Antarct.*
 806 *Sci.*, 16, 517-529, doi:10.1017/S0954102004002299, 2004.
 807 Ma, Y., Bian, L., Xiao, C., Allison, I., and Zhou, X.: Near surface climate of the traverse route from
 808 Zhongshan Station to Dome A, East Antarctica, *Antarct. Sci.*, 22, 443-459,
 809 doi:10.1017/S0954102010000209, 2010.
 810 Marion, G., Farren, R., and Komrowski, A.: Alternative pathways for seawater freezing, *Cold Reg. Sci.*
 811 *Technol.*, 29, 259-266, 1999.
 812 Mayewski, P.A., and Legrand, M.R.: Recent increase in nitrate concentration of Antarctic snow, *Nature*,
 813 346, 258-260, 1990.
 814 McCabe, J.R., Thiemens, M.H., and Savarino, J.: A record of ozone variability in South Pole Antarctic
 815 snow: Role of nitrate oxygen isotopes, *J. Geophys. Res.*, 112, D12303, doi:10.1029/2006JD007822,
 816 2007.
 817 Mulvaney, R., Wagenbach, D., and Wolff, E.W.: Postdepositional change in snowpack nitrate from
 818 observation of year-round near-surface snow in coastal Antarctica, *J. Geophys. Res.*, 103, 11021-11031,
 819 1998.
 820 Mulvaney, R., and Wolff, E.: Evidence for winter/spring denitrification of the stratosphere in the nitrate
 821 record of Antarctic firn cores, *J. Geophys. Res.*, 98, 5213-5220, 1993.
 822 Mulvaney, R., and Wolff, E.: Spatial variability of the major chemistry of the Antarctic ice sheet, *Ann.*
 823 *Glaciol.*, 20, 440-447, 1994.
 824 Parish, T.R., and Bromwich, D.H.: Reexamination of the near-surface airflow over the Antarctic
 825 continent and implications on atmospheric circulations at high southern latitudes, *Mon. Weather. Rev.*,
 826 135, 1961-1973, doi:10.1175/MWR3374.1, 2007.
 827 Pasteris, D., McConnell, J.R., Edwards, R., Isaksson, E., and Albert, M.R.: Acidity decline in Antarctic ice
 828 cores during the Little Ice Age linked to changes in atmospheric nitrate and sea salt concentrations, *J.*
 829 *Geophys. Res.*, 119, 5640-5652, doi:10.1002/2013JD020377, 2014.
 830 Piel, C., Weller, R., Huke, M., and Wagenbach, D.: Atmospheric methane sulfonate and non-sea-salt
 831 sulfate records at the European Project for Ice Coring in Antarctica (EPICA) deep-drilling site in
 832 Dronning Maud Land, Antarctica, *J. Geophys. Res.*, 111, -, 2006.
 833 Qin, D., Zeller, E.J., and Dreschhoff, G.A.: The distribution of nitrate content in the surface snow of the
 834 Antarctic Ice Sheet along the route of the 1990 International Trans-Antarctica Expedition, *J. Geophys.*
 835 *Res.*, 97, 6277-6284, 1992.
 836 Röthlisberger, R., Hutterli, M.A., Sommer, S., Wolff, E.W., and Mulvaney, R.: Factors controlling nitrate
 837 in ice cores: Evidence from the Dome C deep ice core, *J. Geophys. Res.*, 105, 20565-20572, 2000.

838 Röthlisberger, R., Hutterli, M.A., Wolff, E.W., Mulvaney, R., Fischer, H., Bigler, M., Goto-Azuma, K.,
 839 Hansson, M.E., Ruth, U., and Siggaard-Andersen, M.-L.: Nitrate in Greenland and Antarctic ice cores: A
 840 detailed description of post-depositional processes, *Ann. Glaciol.*, 35, 209-216, 2002.
 841 Röthlisberger, R., Mulvaney, R., Wolff, E.W., Hutterli, M.A., Bigler, M., De Angelis, M., Hansson, M.E.,
 842 Steffensen, J.P., and Udisti, R.: Limited dechlorination of sea-salt aerosols during the last glacial period:
 843 Evidence from the European Project for Ice Coring in Antarctica (EPICA) Dome C ice core, *J. Geophys.*
 844 *Res.*, 108, 4526, doi:4510.1029/2003JD003604, 2003.
 845 Rankin, A.M., and Wolff, E.W.: A year-long record of size-segregated aerosol composition at Halley,
 846 Antarctica, *J. Geophys. Res.*, 108, -, 2003.
 847 Rankin, A.M., Wolff, E.W., and Martin, S.: Frost flowers: Implications for tropospheric chemistry and ice
 848 core interpretation, *J. Geophys. Res.*, 107, AAC 4-1–AAC 4-15, 2002.
 849 Russell, A., McGregor, G., and Marshall, G.: 340 years of atmospheric circulation characteristics
 850 reconstructed from an eastern Antarctic Peninsula ice core, *Geophys. Res. Lett.*, 33, L08702,
 851 doi:08710.01029/02006GL025899, 2006.
 852 Russell, A., McGregor, G.R., and Marshall, G.J.: An examination of the precipitation delivery
 853 mechanisms for Dolleman Island, eastern Antarctic Peninsula, *Tellus Series A-dynamic Meteorology &*
 854 *Oceanography*, 56, 501–513, 2004.
 855 Savarino, J., Kaiser, J., Morin, S., Sigman, D.M., and Thieme, M.H.: Nitrogen and oxygen isotopic
 856 constraints on the origin of atmospheric nitrate in coastal Antarctica, *Atmos. Chem. Phys.*, 7,
 857 1925-1945, 2007.
 858 Seinfeld, J.H., and Pandis, S.N., 1997. *Atmospheric Chemistry and Physics: From Air Pollution to*
 859 *Climate Change*, 2nd ed. Wiley, New York.
 860 Shi, G., Buffen, A.M., Hastings, M.G., Li, C., Ma, H., Li, Y., Sun, B., An, C., and Jiang, S.: Investigation of
 861 post-depositional processing of nitrate in East Antarctic snow: isotopic constraints on photolytic loss,
 862 re-oxidation, and source inputs, *Atmos. Chem. Phys.*, 15, 9435–9453, doi:10.5194/acp-15-9435-2015,
 863 2015.
 864 Shi, G., Li, Y., Jiang, S., An, C., Ma, H., Sun, B., and Wang, Y.: Large-scale spatial variability of major ions
 865 in the atmospheric wet deposition along the China Antarctica transect (31° N~ 69° S), *Tellus B*, 64,
 866 17134, doi:10.3402/tellusb.v64i0.17134, 2012.
 867 Shrestha, A., Wake, C., Dibb, J., and Whitlow, S.: Aerosol and Precipitation Chemistry at a Remote
 868 Himalayan Site in Nepal, *Aerosol Science & Technology*, 36, 441-456, 2002.
 869 Sigl, M., Fudge, T.J., Winstrup, M., Coledai, J., Ferris, D., McConnell, J.R., Taylor, K.C., Welten, K.C.,
 870 Woodruff, T.E., and Adolphi, F.: The WAIS Divide deep ice core WD2014 chronology - Part 2:
 871 Annual-layer counting (0-31 ka BP), *Clim. Past*, 11, 3425-3474, 2016.
 872 Smart, D.F., Shea, M.A., Melott, A.L., and Laird, C.M.: Low time resolution analysis of polar ice cores
 873 cannot detect impulsive nitrate events, *Journal of Geophysical Research: Space Physics*, 119,
 874 9430-9440, doi:10.1002/2014JA020378, 2014.
 875 Traversi, R., Becagli, S., Brogioni, M., Caiazzo, L., Ciardini, V., Giardi, F., Legrand, M., Macelloni, G.,
 876 Petkov, B., Preunkert, S., Scarchilli, C., Severi, M., Vitale, V., and Udisti, R.: Multi-year record of
 877 atmospheric and snow surface nitrate in the central Antarctic plateau, *Chemosphere*, 172, 341-354,
 878 doi:10.1016/j.chemosphere.2016.12.143, 2017.
 879 Traversi, R., Becagli, S., Castellano, E., Cerri, O., Morganti, A., Severi, M., and Udisti, R.: Study of Dome
 880 C site (East Antarctica) variability by comparing chemical stratigraphies, *Microchem. J.*, 92, 7-14,
 881 doi:10.1016/j.microc.2008.08.007, 2009.

882 Traversi, R., Udisti, R., Frosini, D., Becagli, S., Ciardini, V., Funke, B., Lanconelli, C., Petkov, B., Scarchilli,
883 C., and Severi, M.: Insights on nitrate sources at Dome C (East Antarctic Plateau) from multi-year
884 aerosol and snow records, *Tellus B*, 66, 22550, doi:10.3402/tellusb.v66.22550, 2014.

885 Traversi, R., Usoskin, I., Solanki, S., Becagli, S., Frezzotti, M., Severi, M., Stenni, B., and Udisti, R.:
886 Nitrate in Polar Ice: A New Tracer of Solar Variability, *Sol. Phys.*, 280, 237-254, 2012.

887 Udisti, R., Becagli, S., Benassai, S., Castellano, E., Fattori, I., Innocenti, M., Migliori, A., and Traversi, R.:
888 Atmospheresnow interaction by a comparison between aerosol and uppermost snow-layers
889 composition at Dome C, East Antarctica, *Ann. Glaciol.*, 39, 53-61, 2004.

890 Wagenbach, D., Ducroz, F., Mulvaney, R., Keck, L., Minikin, A., Legrand, M., Hall, J.S., and Wolff, E.W.:
891 Sea-salt aerosol in coastal Antarctic regions, *J. Geophys. Res.*, 103, 10961-10974, 1998a.

892 Wagenbach, D., Graf, V., Minikin, A., Trefzer, U., Kipfstuhl, J., Oerter, H., and Blindow, N.:
893 Reconnaissance of chemical and isotopic firn properties on top of Berkner Island, Antarctica, *Ann.*
894 *Glaciol.*, 20, 307-312, 1994.

895 Wagenbach, D., Legrand, M., Fischer, H., Pichlmayer, F., and Wolff, E.W.: Atmospheric near-surface
896 nitrate at coastal Antarctic sites, *J. Geophys. Res.*, 103, 11007-11020, 1998b.

897 Warren, S.G., Brandt, R.E., and Grenfell, T.C.: Visible and near-ultraviolet absorption spectrum of ice
898 from transmission of solar radiation into snow, *Appl. Optics*, 45, 5320-5334, 2006.

899 Weller, R., Traufetter, F., Fischer, H., Oerter, H., Piel, C., and Miller, H.: Postdepositional losses of
900 methane sulfonate, nitrate, and chloride at the European Project for Ice Coring in Antarctica
901 deep-drilling site in Dronning Maud Land, Antarctica, *J. Geophys. Res.*, 109, 1-9,
902 doi:10.1029/2003JD004189, 2004.

903 Weller, R., and Wagenbach, D., 2007. Year-round chemical aerosol records in continental Antarctica
904 obtained by automatic samplings.

905 Witherow, R.A., Lyons, W.B., Bertler, N.A., Welch, K.A., Mayewski, P.A., Sneed, S.B., Nysten, T., Handley,
906 M.J., and Fountain, A.: The aeolian flux of calcium, chloride and nitrate to the McMurdo Dry Valleys
907 landscape: evidence from snow pit analysis, *Antarct. Sci.*, 18, 497-505,
908 doi:10.1017/S095410200600054X, 2006.

909 Wolff, E.W., 1995. Nitrate in polar ice, in: Delmas, R.J. (Ed.), in *Ice core studies of global*
910 *biogeochemical cycles*. Springer, New York, pp. 195-224.

911 Wolff, E.W., Barbante, S., Becagle, S., Bigler, M., Boutron, C.F., Castellano, E., de Angelis, M., and
912 Federer, U.: Changes in environment over the last 800,000 years from chemical analysis of the EPICA
913 Dome C ice core, *Quaternary Sci. Rev.*, 29, 285-295, 2010.

914 Wolff, E.W., Bigler, M., Curran, M., Dibb, J., Frey, M., Legrand, M., and McConnell, J.: The Carrington
915 event not observed in most ice core nitrate records, *Geophys. Res. Lett.*, 39, L08503,
916 doi:10.1029/2012GL051603, 2012.

917 Wolff, E.W., Bigler, M., Curran, M.A.J., Dibb, J.E., Frey, M.M., Legrand, M., and McConnell, J.R.:
918 Comment on "Low time resolution analysis of polar ice cores cannot detect impulsive nitrate events"
919 by D.F. Smart et al, *J. Geophys. Res.*, 121, 1920-1924, 2016.

920 Wolff, E.W., Jones, A.E., Bauguitte, S.-B., and Salmon, R.A.: The interpretation of spikes and trends in
921 concentration of nitrate in polar ice cores, based on evidence from snow and atmospheric
922 measurements, *Atmos. Chem. Phys.*, 8, 5627-5634, 2008.

923 Xiao, C., Mayewski, P.A., Qin, D., Li, Z., Zhang, M., and Yan, Y.: Sea level pressure variability over the
924 southern Indian Ocean inferred from a glaciochemical record in Princess Elizabeth Land, east
925 Antarctica, *J. Geophys. Res.*, 109, doi:10.1029/2003JD004065, 2004.

926 Zatko, M., Grenfell, T., Alexander, B., Doherty, S., Thomas, J., and Yang, X.: The influence of snow grain
927 size and impurities on the vertical profiles of actinic flux and associated NO_x emissions on the
928 Antarctic and Greenland ice sheets, *Atmos. Chem. Phys.*, 13, 3547-3567,
929 doi:10.5194/acp-13-3547-2013, 2013.

930 Zatko, M.C., Geng, L., Alexander, B., Sofen, E.D., and Klein, K.: The impact of snow nitrate photolysis on
931 boundary layer chemistry and the recycling and redistribution of reactive nitrogen across Antarctica
932 and Greenland in a global chemical transport model, *Atmos. Chem. Phys.*, 16, 2819-2842,
933 doi:10.5194/acp-16-2819-2016, 2016.

934 Zeller, E.J., Dreschhoff, G.A., and Laird, C.M.: Nitrate flux on the Ross Ice Shelf, Antarctica and its
935 relation to solar cosmic rays, *Geophys. Res. Lett.*, 13, 1264-1267, 1986.

936

937

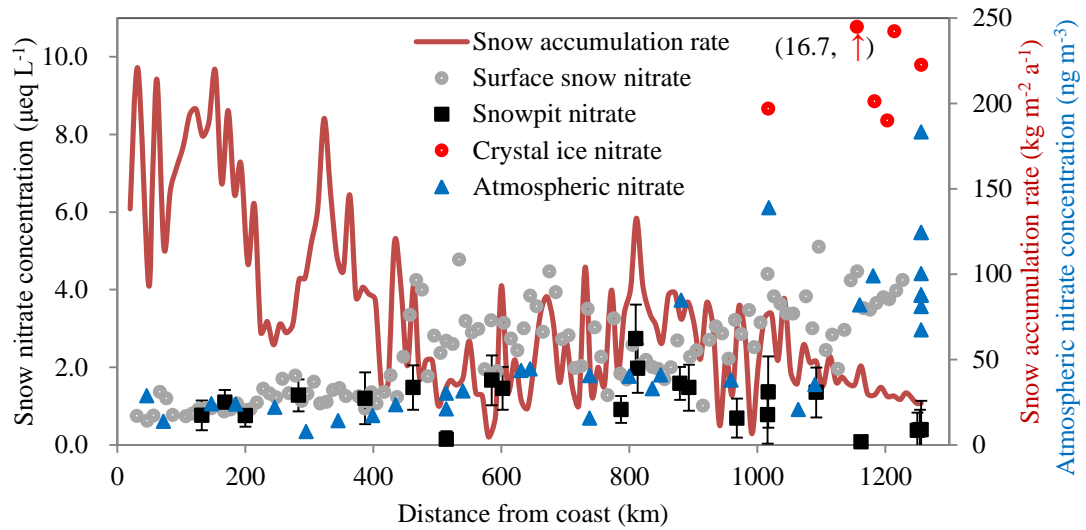
Table 1. Snowpit information on the traverse from coastal Zhongshan Station to Dome A, East Antarctica.

Snowpit No.	Latitude, °	Longitude, °	Elevation, m	Distance to coast, km	Annual snow accumulation, $\text{kg m}^{-2} \text{a}^{-1}$)	Depth, cm	Sampling resolution, cm	Sampling year
SP1	-70.52	76.83	1613	132	193.2	150	5.0	2010/2011
SP2	-71.13	77.31	2037	200	172.0	150	3.0	2012/2013
SP3	-71.81	77.89	2295	283	99.4	200	5.0	2012/2013
SP4	-72.73	77.45	2489	387	98.3	200	5.0	2012/2013
SP5	-73.40	77.00	2545	452	90.7	200	5.0	2012/2013
SP6	-73.86	76.98	2627	514	24.6	300	2.5	2012/2013
SP7	-74.50	77.03	2696	585	29.2	100	2.0	2012/2013
SP8	-74.65	77.01	2734	602	80.2	180	2.0	2010/2011
SP9	-76.29	77.03	2843	787	54.8	200	2.0	2012/2013
SP10	-76.54	77.02	2815	810	100.7	240	3.0	2010/2011
SP11	-77.13	76.98	2928	879	81.2	200	2.5	2012/2013
SP12	-77.26	76.96	2962	893	83.4	265	5.0	2009/2010
SP13	-77.91	77.13	3154	968	33.3	200	2.0	2012/2013
SP14	-78.34	77.00	3368	1015	87.6	216	3.0	2010/2011
SP15	-78.35	77.00	3366	1017	70.0	162	2.0	2009/2010
SP16	-79.02	76.98	3738	1092	25.4	200	2.5	2012/2013
SP17	-79.65	77.21	3969	1162	46.2	130	2.0	2010/2011
SP18	-80.40	77.15	4093	1250	24.2	300	2.0	2010/2011
SP19	-80.41	77.11	4092	1254	23.7	300	1.0	2009/2010
SP20	-80.42	77.12	4093	1256	23.5	300	2.5	2012/2013
Core 1 ²⁾	-70.83	77.08	1850	168	127.0	-	-	1996/1997
Core 2 ³⁾	-76.53	77.03	2814	813	101.0	-	-	1998/1999

1) Annual snow accumulation rate is obtained from the field bamboo stick measurements (2009 - 2013), updated from the report (Ding et al., 2011). Note that snow accumulation rate at the two ice core sites are derived from ice core measurements.

2) Core 1, ice core data of previous report (Li et al., 1999; Xiao et al., 2004).

3) Core 2, ice core data of previous report (Li et al., 2009).



947

948 **Figure 1.** Concentrations of NO_3^- in snow (surface snow, crystal ice and snowpits; on the primary
949 y-axis) and atmosphere (on the secondary y-axis), with error bars representing one standard deviation
950 of NO_3^- (1σ) for individual snowpits. Also shown is the annual snow accumulation rate on the traverse
951 (red solid line; based on Ding et al. (2011)). Note that NO_3^- concentration in one crystal ice sample (red
952 dot) is higher than the maximum value of the primary y-axis (NO_3^- concentration = $16.7 \mu\text{eq L}^{-1}$ in the
953 parentheses).

954

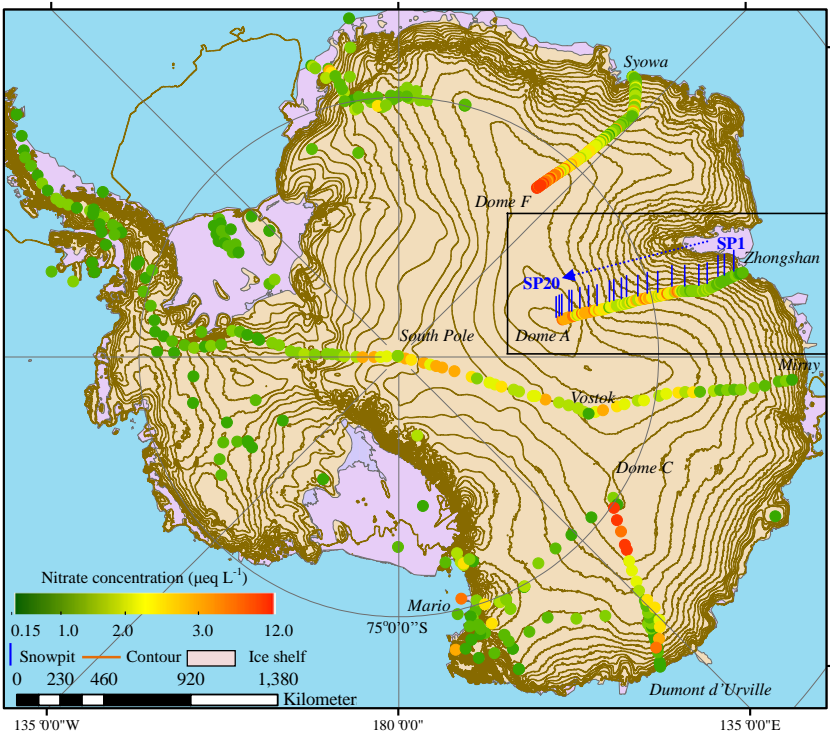


Figure 2. Concentrations of NO_3^- in surface snow across Antarctica. Note that the values of crystal ice around Dome A were not included. The data of DDU to Dome C is from Frey et al. (2009). The other surface snow NO_3^- concentrations are from compiled data (Bertler et al., 2005 and references therein). Also illustrated are the locations of snowpits on the traverse route from Zhongshan to Dome A in this study (SP1 to SP20, solid short blue line; Table 1).

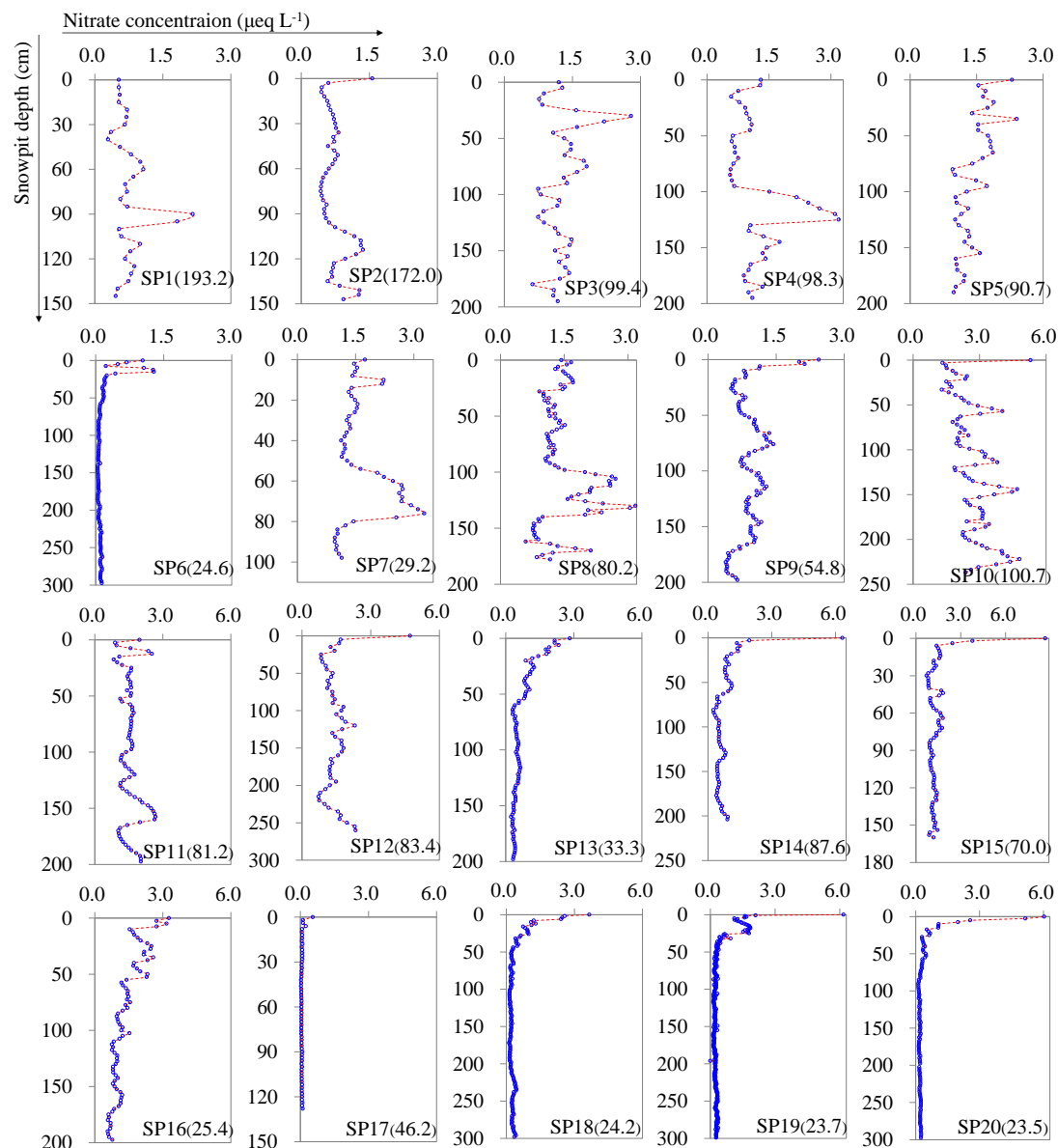
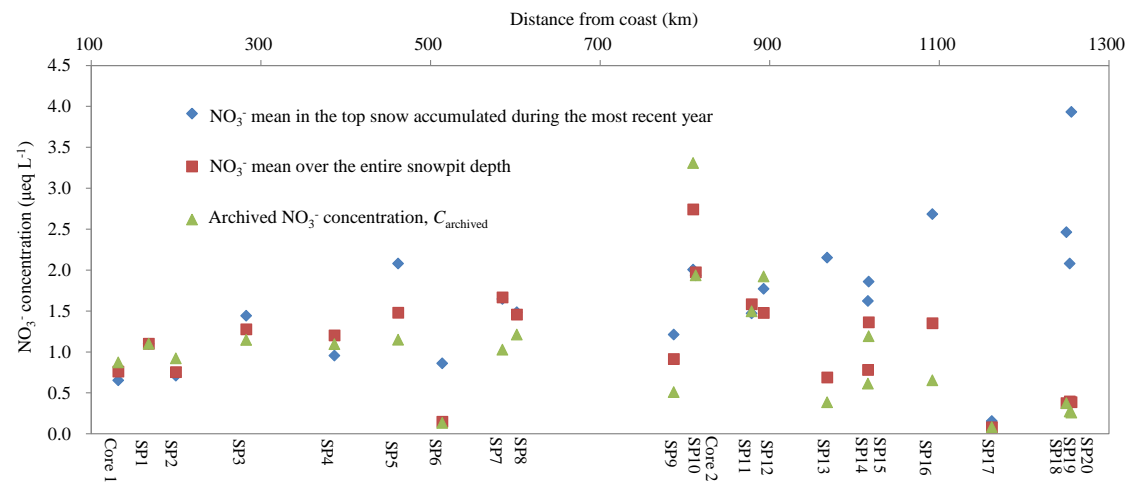


Figure 3. The full profiles of NO_3^- concentrations for snowpits collected on the traverse from the coast to Dome A, East Antarctica (SP1 is closest the coast; SP20 the furthest inland; see Figure 2). The details on sampling of the snowpits refer to Table 1. The numbers in parentheses in each panel denote the annual snow accumulation rates ($\text{kg m}^{-2} \text{a}^{-1}$). Note that the scales of x-axes for the snowpits SP1 – SP9 and SP10 – SP20 are different.

971



972

973 **Figure 4.** Mean concentrations of NO_3^- for the entire snowpit depth (in square), the uppermost layer

974 covering one-year snow accumulation (in diamond) and the bottom layer covering a full annual cycle

975 of deposition (archived NO_3^- concentration, C_{archived} , in triangle).

976

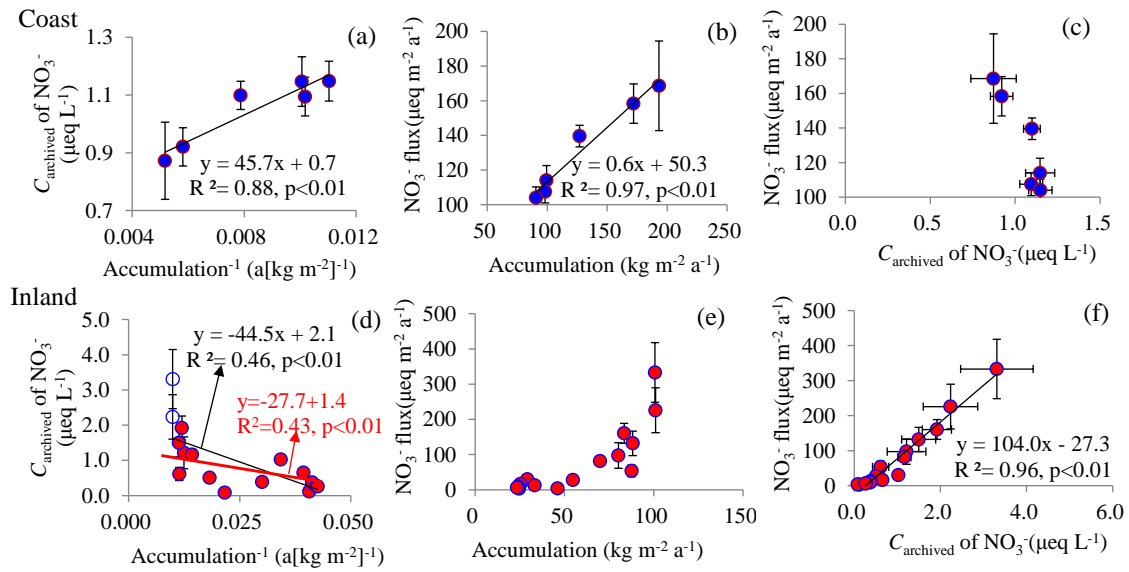


Figure 5. The relationships amongst snow accumulation rate, the archived concentration (C_{archived}), and flux of NO_3^- in coastal (top row, (a), (b) and (c)) and inland (bottom row, (d), (e) and (f)) Antarctica. In panel (d), the linear fit in black line ($y = -44.5x + 2.1$) includes the full data set, while the linear equation in red ($y = -27.7x + 1.5$) was obtained by excluding two cases (open circles) with snow accumulation rate larger than $100 \text{ kg m}^{-2} \text{a}^{-1}$ (see the main text). The flux values are the product of C_{archived} of NO_3^- and snow accumulation rate, namely the archived flux. Least squares regressions are noted with solid lines and are significant at $p < 0.01$. Error bars represent one standard deviation (1σ).

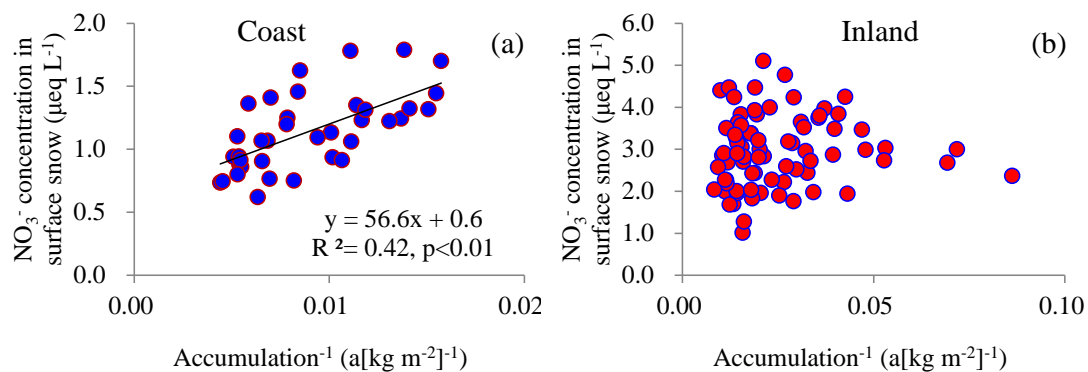
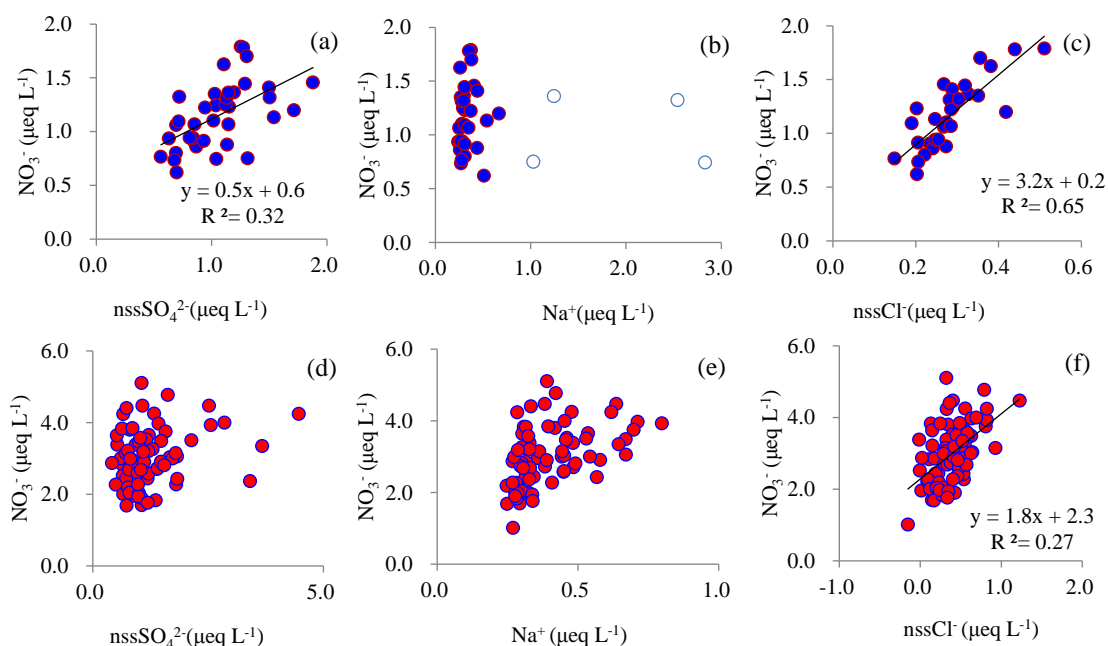


Figure 6. The relationships between NO_3^- concentration and inverse snow accumulation rate in surface snow in coastal (panel (a)) and inland (panel (b)) Antarctica. Least squares regressions are noted with solid line and are significant at $p < 0.01$.

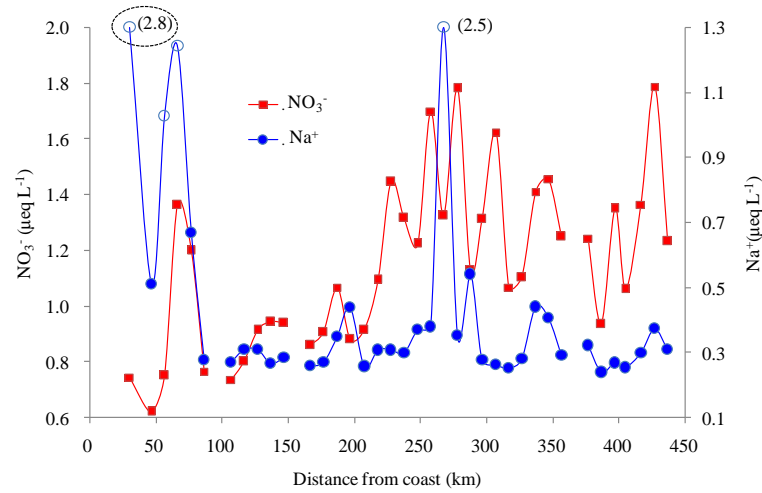
994



995

996 **Figure 7.** Relationships between NO_3^- and co-existing major ions in surface snow in coastal (top row,
 997 (a), (b) and (c)) and inland (bottom row, (d), (e) and (f)) Antarctica. Least squares regressions are noted
 998 with solid line and are significant at $p < 0.01$. The 4 samples with high Na^+ concentrations are denoted
 999 by blue open circles (b), the same as those in Figure 8 (the blue open circles). Note that the 4 samples
 1000 were excluded in the plot of NO_3^- vs. nssCl^- (c).
 1001

1002



1003

1004

1005

1006

1007

1008

1009

Figure 8. Concentrations of NO_3^- and Na^+ in surface snow samples on the coast. Four samples with high Na^+ concentrations are denoted by open circles, corresponding to those in Fig. 7b. Note that Na^+ concentrations in two samples, 2.5 and 2.8 $\mu\text{eq L}^{-1}$ in parentheses, are above the maximum value of the secondary y-axis (Na^+ concentration). The sample in the dashed ellipse, with Na^+ concentration of 2.8 $\mu\text{eq L}^{-1}$, is the fresh snowfall.